Comparison of bubbles interaction mechanisms of two-group Interfacial Area Transport Equation model

E.V. Kuidjo Kuidjo, M.G. Rodio, R. Abgrall, P. Sagaut

Comparison of bubbles interaction mechanisms of two-group Interfacial Area Transport Equation model

E.V. Kuidjo Kuidjo [a], M.G. Rodio [a,*], R. Abgrall [b], P. Sagaut [c]

[a] Université Paris-Saclay, CEA, Service de Thermo-hydraulique et de Mécanique des Fluides, 91191, Gif-sur-Yvette, France
[b] University of Zürich, Institute of Mathematics, Winterthurerstrasse 190 CH-8057 Zürich, Switzerland
[c] M2P2, UMR7340, Centrale Marseille, Plot 6, 38 rue Joliot-Curie, 13451 Marseille, France

ARTICLE INFO

Keywords:
Two-group interfacial area transport equation (IATE)
Two-fluid model
CFD
Churn regime
Cap-turbulent regime
Bubbly regime

ABSTRACT

This work deals with 3D simulations of complex bubbly, cap-bubbly and churn regimes exhibiting bubbles of different shapes and with broad bubble size distribution. The first contribution of this work is to investigate and compare several bubble interaction mechanisms of coalescence and fragmentation for the 2-Group Interfacial Area Transport Equation (IATE) model. For two of these models, this is the first time their performances are assessed within a CFD code. The second contribution is to propose and assess a novel model of fragmentation and coalescence. Finally, a validation versus experimental data on three different configurations and three different regimes is performed. In particular, the interaction mechanisms are analysed for one specific regime. The implementation of the two-group IATE model has been systematically performed in the 3D NEPTUNE CFD code.

1. Introduction

Two-phase gas–liquid flows are encountered in nature (ocean waves, river flooding, for example) and several industrial machines and processes such as nuclear power plants, processing industries, heat transfer systems, transport systems. In the nuclear industry, two-phase vapour–liquid flows may appear in the primary loop of Pressurized Water Reactors (PWR) during some accident scenarios. The cooling system break accident is an example. During this kind of accident, coolant loss leads to an increase in temperature, inducing partial evaporation of the liquid phase and the appearance of a vapour–liquid flow in the reactor vessel and/or in the loops. Such scenarios need to be studied and understood to prevent their occurrence and guarantee nuclear reactor safeness under these conditions. Specifically, this problem requires a good understanding of the mechanics of two-phase flows under a wide range of conditions.

In these scenarios, three main regimes can be typically distinguished: bubbly, mixed or transitional, and separated or stratified (Ishii and Hibiki, 2006). In these regimes, gas bubbles may take an infinite number of shapes and sizes that influence how the fluid flow transports them and how the interaction mechanisms (coalescence/breakup) come into play.

The bubbly regime, as well as the stratified one, have been largely investigated in the literature (Bois, 2017; du Cluzeau et al., 2019, 2020b,a). On the contrary, fewer works exist on transitional and mixed regimes, which is the focus of this paper.

The transitional regimes can be reproduced using an Euler–Euler approach, with three balance equations (mass, momentum and energy), for each phase. Their momentum exchanges are expressed as the sum of several interfacial forces, proportional to two crucial parameters: the Interfacial Area Concentration (IAC), a_i, and the bubble diameter. This last one is, usually, described by the *Sauter mean diameter* D_{sm} classically expressed as:

$$D_{sm} = \frac{6\alpha}{a_i}, \tag{1}$$

see Ishii and Hibiki (2006) for more details. The most straightforward approach proposed in the literature is to consider a fixed diameter corresponding to the Sauter mean diameter to estimate the IAC using relation (1). This mono-dispersed approach is suitable only for the bubbly flow regime with a very low void fraction for which robust formulations of the interfacial forces have been developed (Frank et al., 2008). The limit of this approach is to force no interaction between bubbles, thus neglecting the bubble size distribution in the flow. However, when this hypothesis is not respected, the fixed morphology approach fails to predict the spatial development of the flow (Krepper et al., 2005). Few approaches have been proposed to consider the polydispersity in the framework of the Euler–Euler two-fluid model.

* Corresponding author.
E-mail address: mariagiovanna.rodio@cea.fr (M.G. Rodio).

The most popular methods are the Population Balance Model (PBM), as the MUltiple SIze Group (iMUSIG) model (Krepper et al., 2009, 2008) , and the Interfacial Area Transport Equation (IATE) model (Kocamustafaogullari and Ishii, 1995; Hibiki and Ishii, 2000). We encourage the reading of Wang and Ishii (2021), Kim et al. (2021) and Liu et al. (2015) for more details.

In this paper, we are interested in the last approach and, in particular, in the two-group IATE method that proposes a separation of bubbles into small bubbles (Group-1) and large ones (Group-2). In this case, two interfacial area transport equations are solved. These two equations provide the coalescence and breakup interaction mechanisms as source/sink terms. The choice of this model was motivated by the fact that compared to the IATE one-group approach, in which a single group of bubbles is modelled, the IATE 2-groups model improves the coalescence and breakup mechanisms between the gas and the liquid and proposes the same mechanisms between the two groups of bubbles (Hibiki and Ishii, 2000; Fu and Ishii, 2003; Sun et al., 2004a). Modelling two groups of bubbles also allows considering two different velocities between the two groups of bubbles. In the particular conditions of a flow in a channel, this distinction would allow, for example, to differentiate the behaviour of small bubbles that tend to approach the wall from that of large bubbles that tend to migrate towards the middle of the channel (see Tomiyama et al., 2002). Compared with the iMUSIG, the method is limited to only two groups of bubbles, but the strength of this choice is that validation is less complex than for a larger number of groups of bubbles.

When considering the IATE method, the most crucial challenge is to construct appropriate closure relations of bubble–bubble interactions capable of reproducing specific flow regimes. A recent review proposed in Kim et al. (2021) shows that a few sets of coalescence/break-up terms have been proposed for the two-group IATE model in adiabatic conditions. Each of these models was exclusively developed and validated through experimental measurements of interfacial area concentration acquired in single or multiple configurations. In 2001, Sun (2001) (and later in 2004 Sun et al., 2004a) developed a set of two-group source-term models for flows in confined channels. The model was subsequently tested in 2013 for reproducing experimental configurations under high pressure (greater than 580 kPa) in Ozar et al. (2013), and it was improved for reproducing 8 × 8 rod bundle geometries in Yang et al. (2016). In the same years, in Fu and Ishii (2003), the authors proposed a two-group model for small-diameter circular channels, which was later improved in Doup (2014) and Worosz (2015). Both studies illustrated a clear need to improve the source terms of coalescence and break-up, particularly for Group-2. In 2012, in Smith et al. (2012a), the authors proposed the interaction models for the two-group bubbles for large-diameter vertical channels. In Schlegel et al. (2015), they used the model of Smith et al. (2012a), proposing optimized coefficients on a more extensive database. Recently, in Wang and Ishii (2021), the authors have compared three different interaction mechanism models (Fu and Ishii, 2003; Worosz, 2015; Sun et al., 2004a) with respect to the database coming from the Sun's experimental campaign. They showed that the Sun model is the best, even if it generates a non-negligible error in some examined configurations. Moreover, they proposed a new formulation of the Wake Entrainment (WE) term since previous studies recognize this mechanism as the major mechanism for the bubbly to slug transition.

A final significant point to note is that only the Sun model (Sun et al., 2004a) has been implemented and used in CFD simulations (Lee et al., 2013; Sharma et al., 2019). In our opinion, only a detailed CFD simulation can thoroughly validate these models, allowing us to observe the complete interactions between the various mechanisms and allowing comparison with both interfacial area profiles and variables describing flow dynamics evolution, such as phase's velocity or volume fraction, which are extremely important.

The first contribution of this paper is to compare four Coalescence/Break-up (C/B) models (including the novel proposed model), implemented in a CFD code and assessed on several configurations. Models chosen for this analysis are the following ones: Sun et al. (2004c), Smith et al. (2012a) and Schlegel et al. (2015) and a novel one that will be referred later as SMITH-SUN. Note that in the literature, SMITH, SCHLEGER have never been used before within a CFD code, and for SMITH-SUN, this is the first time ever. The 3D CFD code chosen for comparison is NEPTUNE_CFD (EDF et al.; Coste, 2013). The second contribution of this paper is to propose a novel C/B model by combining the formulation of the coalescence and break-up terms proposed by Smith et al. (2012a) with the coefficients proposed in Sun et al. (2004c). The ratio for this choice comes from empirical considerations on the evolution of the source/sink terms. More details are provided in Section 2.3.2.

Finally, the third contribution is the validation of numerical predictions against the experimental data on three different configurations and regimes: (i) a confined rectangular section (Sun et al., 2004a), (ii) a small diameter pipe (Liu and Bankoff, 1993) and (iii) a large diameter pipe (Schaffrath et al., 2001). Three different regimes are investigated, *i.e.* bubbly, cap-turbulent and churn. This validation study is particularly relevant because it allows illustrating the limitations of the four models examined, and highlighting the interest in using the novel model proposed here, *i.e.* SMITH-SUN, by showing the validity and limitations of this choice.

Exclusively for the Sun's experiment, an analysis and comparison of C/B interaction mechanisms, for the four models, is proposed with the aim to identify which mechanism is dominant in the simulation and the limitations of each model.

This paper is organized as follows. In Section 2, the mathematical model used for all simulations is described. In particular, it includes the IATE model (described in 2.1), the three-field model (described in 2.2) and the source terms used to close the system 2.3. Section 3 is dedicated to the description of the numerical schemes used in this paper. Finally, Section 4 presents the results of the simulations of cap-bubbly and churn-turbulent regimes. Conclusions and perspectives follow.

2. Mathematical model

Let us detail the equations that we solve in the code. As mentioned previously, each phase is represented by a set of two balance equations (the mass and momentum equations). In this paper, we developed them in NEPTUNE_CFD (it is a CFD code jointly developed by EDF, CEA, FRAMATOME and IRSN EDF et al.), but the equations described in this section are independent from the code. The balance equations introduce the volume fraction, the density and the velocity of each phase k (α_k, ρ_k and v_k), as unknowns of the system.

Their source terms (terms on the right-hand side of the equations), which describe the interfacial forces, $\mathbf{M}_{l\to g1}$, and the mass transfers between the bubbles, $\Delta\dot{m}_{g1\to g2}$, introduce another unknown: the interfacial area a_i, for each phase. So to close the system, it is necessary to solve two more transport equations for a_i (see Eqs. (4) and (6) and the source/sink terms in Section 2.3.2) and to model $M_{lg,k}$ (see Eq. (17) and Appendix A).

2.1. Two-group Interfacial Area Transport Equation (IATE)

The two-group IATE model aims at handling polydispersity in mixed regimes, including cap-bubbly and churn-turbulent flows. It predicts dynamically the change in the interfacial area concentration (IAC) of each group of bubbles by means of two transport equations. In this approach, five types of bubbles are categorized into two groups: the Group-1 includes spherical and distorted bubbles, while Group-2 includes cap, slug and churn-turbulent bubbles. The threshold between the two groups is determined by the maximum distorted bubble limit or critical diameter D_c proposed by Ishii and Zuber (1979) as

$$D_c = 4\sqrt{\frac{\sigma}{g\Delta\rho}} \tag{2}$$

where σ is the surface tension, g is the gravitational acceleration and $\Delta\rho$ is the difference between the liquid and gas densities.

Starting from the Boltzmann equation and by means of an averaging process, Ishii et al. (2002) derived two transport equations for the interfacial area concentration of each group:

$$\frac{\partial a_{i1}}{\partial t} + \nabla\cdot(a_{i1}\mathbf{v}_{gi1}) = \frac{2}{3}\frac{a_{i1}}{\alpha_{g1}}\left[\frac{\partial \alpha_{g1}}{\partial t} + \nabla.(\alpha_{g1}\mathbf{v}_{g1}) - \eta_{ph1}\right] + \tag{3}$$

$$- \chi(D^*_{c1})^2\frac{a_{i1}}{\alpha_{g1}}\left[\frac{\partial \alpha_{g1}}{\partial t} + \nabla.(\alpha_{g1}\mathbf{v}_{g1}) - \eta_{ph1}\right] + \sum_j \phi_{j,1} + \phi_{ph1} \tag{4}$$

$$\frac{\partial a_{i2}}{\partial t} + \nabla\cdot(a_{i2}\mathbf{v}_{gi2}) = \frac{2}{3}\frac{a_{i2}}{\alpha_{g2}}\left[\frac{\partial \alpha_{g2}}{\partial t} + \nabla.(\alpha_{g2}\mathbf{v}_{g2}) - \eta_{ph2}\right] + \tag{5}$$

$$+ \chi(D^*_{c1})^2\frac{a_{i1}}{\alpha_{g1}}\left[\frac{\partial \alpha_{g1}}{\partial t} + \nabla.(\alpha_{g1}\mathbf{v}_{g1}) - \eta_{ph1}\right] + \sum_j \phi_{j,2} + \phi_{ph2} \tag{6}$$

where the subscripts 1 and 2 stand for the Group-1 and Group-2 bubbles respectively. We have set $D^*_{c1} = D_c/D_{sm1}$, $\mathbf{v}_{gi}$ is the interfacial velocity, α_g is the void fraction and $\mathbf{v}_g$ is the gas phase centre mass velocity. The coefficient χ accounts for the inter-group void transport at the boundary due to expansion and compression, D_{sm1} is the Sauter mean diameter for Group-1 bubbles, ϕ_j and ϕ_{ph} are the interfacial area source/sink rate due to the bubble interactions and the phase change respectively, where the subscript $j = 1, 2$. The rate of volume generated by nucleation source per unit mixture volume is η_{ph}. For an isothermal flow, the terms $\phi_{ph,i}$ and $\eta_{ph,i}$ (with i = 1,2) are null. In this study, the interfacial gas velocity $\mathbf{v}_{gi}$ is approximated by the gas phase centre mass velocity $\mathbf{v}_g$. In order to close the IATE model, the source/sink terms should be established through the mechanistic modelling of bubble interactions and nucleation/condensation processes if any.

2.2. The three-field two-fluid model

The two-group IATE model requires a velocity field for each bubble group as well as a volume fraction. Within the Euler framework, Group-1 bubbles and Group-2 bubbles are treated as two Euler fields with each having its own continuity and momentum equation. Including the Euler field representing the liquid phase, this leads to a three-field model (Sun et al., 2004b):

$$\frac{\partial(\alpha_{g1}\rho_g)}{\partial t} + \nabla.\left(\alpha_{g1}\rho_g\mathbf{v}_{g1}\right) = \Gamma_{l\to g1} - \Delta\dot{m}_{g1\to g2} \tag{7}$$

$$\frac{\partial(\alpha_{g2}\rho_g)}{\partial t} + \nabla.\left(\alpha_{g2}\rho_g\mathbf{v}_{g2}\right) = \Gamma_{l\to g2} + \Delta\dot{m}_{g1\to g2} \tag{8}$$

$$\frac{\partial\left(\alpha_l\rho_l\right)}{\partial t} + \nabla.\left(\alpha_l\rho_l\mathbf{v}_l\right) = -\Gamma_{l\to g1} - \Gamma_{l\to g2}. \tag{9}$$

Here, $\Gamma_{l\to g1}$ and $\Gamma_{l\to g2}$ are the mass transfer between the liquid phase and the gas phase for the Group-1 bubbles and for the Group-2 bubbles, respectively. $\Delta\dot{m}_{g1\to g2}$ is the inter-group mass transfer and it is defined as follows (Sun et al., 2004b):

$$\Delta\dot{m}_{g1\to g2} = \rho_g\left[\sum_j \eta_{j,2} + \chi\times(D^*_{c1})^3\left(\frac{\partial\alpha_{g1}}{\partial t} + \nabla.(\alpha_{g1}\mathbf{v}_{g1}) - \eta_{ph1}\right)\right] \tag{10}$$

where $\eta_{j,2}$ is the net inter-group void fraction transport from Group-1 to Group-2 bubbles and η_{phk} is the source/sink term for the gas volume due to evaporation/condensation. The inter-group transfer coefficient is χ and D^*_{c1} is the non-dimensional bubble.

Supposing that the pressure field is the same in each bubble group, interfacial shear is equal to the shear in the bulk phase and interfacial pressure is equal to the pressure in the bulk phase (Sun et al., 2003), the momentum equations can be defined as:

$$\frac{\partial}{\partial t}\left(\alpha_{g1}\rho_g\mathbf{v}_{g1}\right) + \nabla.\left(\alpha_{g1}\rho_g\mathbf{v}_{g1}\mathbf{v}_{g1}\right) = -\alpha_{g1}\nabla p + \nabla.\left[\alpha_{g1}\left(\tau^{\mu}_{g1} + \tau^{T}_{g1}\right)\right]$$

$$+ \alpha_{g1}\rho_g\mathbf{g} \tag{11}$$

$$+ (\Gamma_{l\to g1} - \Delta\dot{m}_{12})\mathbf{v}_{gi1} + \mathbf{M}_{l\to g1} \tag{12}$$

$$\frac{\partial}{\partial t}\left(\alpha_{g2}\rho_g\mathbf{v}_{g2}\right) + \nabla.\left(\alpha_{g2}\rho_g\mathbf{v}_{g2}\mathbf{v}_{g2}\right) = -\alpha_{g2}\nabla p + \nabla.\left[\alpha_{g2}\left(\tau^{\mu}_{g2} + \tau^{T}_{g2}\right)\right]$$

$$+ \alpha_{g2}\rho_g\mathbf{g} \tag{13}$$

$$+ (\Gamma_{l\to g2} + \Delta\dot{m}_{12})\mathbf{v}_{gi2} + \mathbf{M}_{l\to g2} \tag{14}$$

$$\frac{\partial}{\partial t}\left(\alpha_l\rho_l\mathbf{v}_l\right) + \nabla.\left(\alpha_l\rho_l\mathbf{v}_l\mathbf{v}_l\right) = -\alpha_l\nabla p + \nabla.\left[\alpha_l\left(\tau^{\mu}_l + \tau^{T}_l\right)\right] + \alpha_l\rho_l\mathbf{g} \tag{15}$$

$$- (\Gamma_{l\to g1} + \Gamma_{l\to g2})\mathbf{v}_{li} - \mathbf{M}_{l\to g1} - \mathbf{M}_{l\to g2} \tag{16}$$

where $M_{l\to g1}$ and $M_{l\to g2}$ are the interfacial momentum transfer terms for the Group-1 and for the Group-2, respectively. τ^{μ}_l and τ^{T}_l are the viscous and turbulent stress tensor, respectively.

As mentioned in Section 2, the equations system solved in this paper includes the Eqs. (4), (6) and from (7) to (16). So, in order to close it, we need to introduce other terms, which are described in Section 2.3 (see Appendix A, Sun et al. (2004c), Smith et al. (2012b) and Schlegel et al. (2015), too).

2.3. The source terms

2.3.1. Interfacial forces

Usually, the interfacial momentum transfer terms $M_{l\to g1}$ and $M_{l\to g2}$ are expressed as a sum of various averaged forces as follows

$$\mathbf{M}_{l\to gk} = \mathbf{M}^{D}_{l\to gk} + \mathbf{M}^{L}_{l\to gk} + \mathbf{M}^{TD}_{l\to gk} + \mathbf{M}^{AM}_{l\to gk} \qquad k = 1, 2 \tag{17}$$

where $\mathbf{M}^{D}_{l\to gk}$ is the drag force, $\mathbf{M}^{L}_{l\to gk}$ is the lift force, $\mathbf{M}^{TD}_{l\to gk}$ is the turbulent dispersion force, $\mathbf{M}^{AM}_{l\to gk}$ is the added mass force. The expression of each term is given in Appendix A. These interfacial forces are proportional to the interfacial area concentration and/or contain the bubble diameter in their expressions. So, a robust and precise estimation of these two variables is mandatory.

2.3.2. Source/sink terms for two-group IATE

Coalescence and disintegration interaction mechanisms should be modelled as source/sink terms in the interfacial area transport equations. A few sets of source/sink terms exist in the literature. The derivation process of these terms starts with choosing the physical interaction mechanisms to be accounted for, and then a formulation of an empirical expression from the physical analysis of each mechanism is given. This analysis usually depends on the investigated geometry devices. Moreover, the coefficients appearing in the source/sink terms are tuned with respect to an experimental database. A schematic view of these bubble interaction mechanisms is summarized on Fig. 1. Each of these sets of terms accounts for the following five primary bubble interaction mechanisms:

- Random Collision (RC): coalescence through random collision driven by turbulent eddies;
- Wake Entrainment (WE): coalescence through collision due to acceleration of the following particle in the wake of the preceding particle;
- Turbulent Impact (TI): disintegration upon impact of turbulent eddies;
- Shearing-off (SO): shearing-off around the base rim of the cap bubble;
- Surface Instability (SI): break-up of large cap bubble due to surface instability;

In Group-1's and Group-2's interfacial area transport equations, these interactions are accounted for respectively in the terms $\sum_j \phi_{j,1}$ and $\sum_j \phi_{j,2}$. These terms are written as:

$$\sum_j \phi_{j,1} = \phi^{(1)}_{RC} + \phi^{(12,2)}_{RC,1} + \phi^{(1)}_{WE} + \phi^{(12,2)}_{WE,1} + \phi^{(1)}_{TI} + \phi^{(2,1)}_{TI,1} + \phi^{(2,12)}_{SO,1} \tag{18}$$

$$\sum_j \phi_{j,2} = \phi^{(11,2)}_{RC,2} + \phi^{(12,2)}_{RC,2} + \phi^{(2)}_{RC} + \phi^{(11,2)}_{WE,2} + \phi^{(12,2)}_{WE,2} + \phi^{(2)}_{WE} + \phi^{(2)}_{TI,2}$$

$$+ \phi^{(2,12)}_{SO,2} + \phi^{(2)}_{SI} \tag{19}$$

$$\sum_j \eta_{j,2} = \eta^{(11,2)}_{RC,2} + \eta^{(12,2)}_{RC,2} + \eta^{(11,2)}_{WE,2} + \eta^{(12,2)}_{WE,2} + \eta^{(2,12)}_{SO,2} + \eta^{(2,1)}_{TI,2} \tag{20}$$

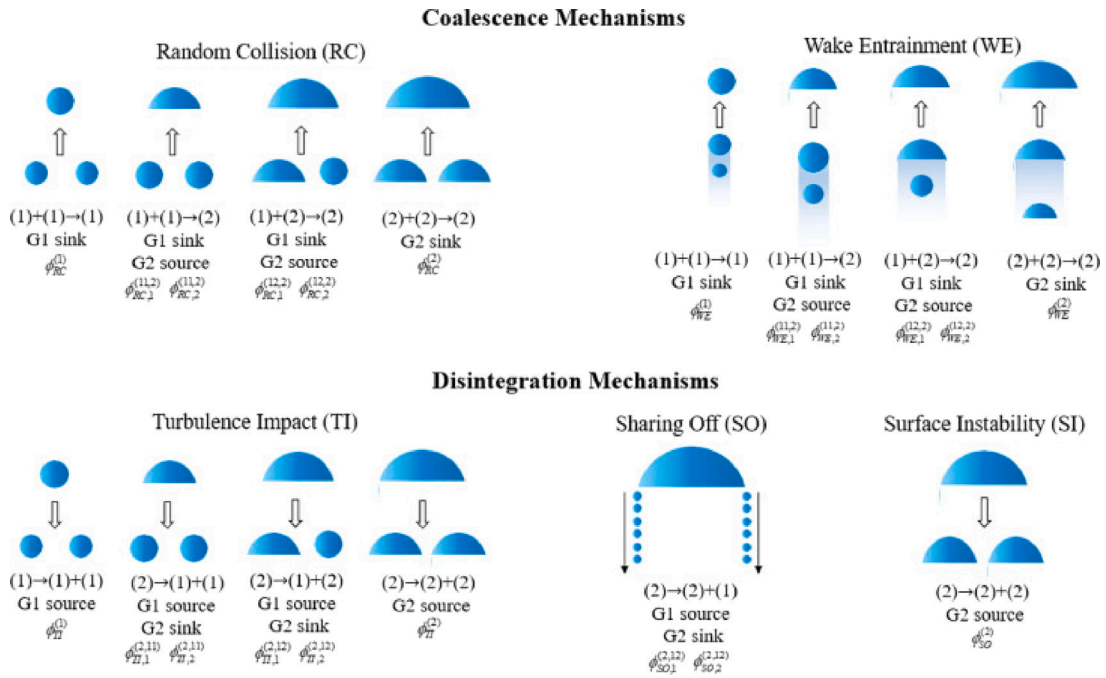

Fig. 1. Schematic illustrations of two-group bubble interactions.
Source: From Wang and Ishii (2021).

Table 1
Summary of the main characteristics of two-group IATE coalescence and breakup models.

Name	Regime	Velocities (m/s)	Configuration D, L, G (mm)
SUN	cap, churn	$j_g < 2.01$; $j_l < 2.84$	Confined rectangular section; $L = 200$; $G = 10$
SMITH	bubbly, cap, churn	$j_g < 8$; $j_l < 2$	Large diameter pipe; $D = 102; 152$
SCHLEGEL	bubbly, cap, churn	$j_g < 11$; $j_l < 2$	Large diameter pipe; $D = 152; 203; 304$

The superscript (ab, c), (with $a, b, c = 1, 2$), indicates the groups which take part in the interaction process: bubbles belonging to Group-a and Group$-b$ interact to form Group$-c$ bubbles. When $a = b = c$, the superscript is replaced by (a). For the sake of clarity, all mathematical expressions of these terms are moved to appendices and detailed for the four models compared in this work. Only main information and differences are discussed hereafter:

Table 1 summarizes the main characteristics of the database used to tune the coefficients appearing in the terms for each model.

- SUN Model (Sun et al., 2004c)
  This set of terms is presented in Sun et al. (2004c). The terms were developed for flows in confined rectangular sections with large aspect ratio. Due to the small gap dimension, Group-2 bubbles are confined between two parallel flat walls. So the wall effect is important. The data used by the authors to tune the coefficients were those of a two-phase upward air–water flow with a test section of 200 mm in width and 10 mm in gap (Sun et al., 2004a) in cap-turbulent and churn-turbulent regimes. The superficial liquid velocity j_f ranges from 0.32 to 2.84 m/s and the superficial gas velocity j_g ranges from 0.39 to 2.01 m/s. SUN coefficients are given in Table 2.
- SMITH Model (Smith et al., 2012a)
  This set of terms is presented in Smith et al. (2012b). The constants that appear in the terms were benchmarked against the data collected by Smith et al. (2012b) in pipes with diameters of 0.102 mm and 0.152 mm and for flows in bubbly, cap-bubbly and churn-turbulent flow conditions. To evaluate the IATE source and sink terms, the model predictions for one-dimensional steady-state cases were analysed. Average errors in interfacial area concentration were 10.2% for the 0.102 m cases and 6.5% for the 0.152 m. SMITH coefficients are given in Table 2.

Table 2
Summary of SUN and SMITH coefficients and constants in source/sink terms of IATE.

Notation	SUN coefficients	SMITH coefficients
$\phi^{(1)}_{RC}$	$C^{(1)}_{RC} = 0.005$	$C^{(1)}_{RC} = 0.01$
$\phi^{(12,2)}_{RC,1}$	$C^{(12,2)}_{RC} = 0.005$	$C^{(12,2)}_{RC} = 0.01$
$\phi^{(11,2)}_{RC,2}$	$C^{(1)}_{RC} = 0.005$	$C^{(1)}_{RC} = 0.01$
$\phi^{(12,2)}_{RC,2}$	$C^{(12,2)}_{RC} = 0.005$	$C^{(12,2)}_{RC} = 0.01$
$\phi^{(2)}_{RC}$	$C^{(2)}_{RC} = 0.005$, $C_{RC2} = 3.0$	$C^{(2)}_{RC} = 0.01$, $C_{RC2} = 3.0$
	$C_{RC1} = 3.0$, $\alpha_{g1,max} = 0.62$	$C_{RC1} = 3.0$, $\alpha_{g1,max} = 0.62$
$\phi^{(1)}_{WE}$	$C^{(1)}_{WE} = 0.002$	$C^{(1)}_{WE} = 0.002$
$\phi^{(12,2)}_{WE,1}$	$C^{(12,2)}_{WE} = 0.002$	$C^{(12,2)}_{WE} = 0.01$
$\phi^{(11,2)}_{WE,2}$	$C^{(11,2)}_{WE} = 0.002$	$C^{(11,2)}_{WE} = 0.01$
$\phi^{(12,2)}_{WE,2}$	$C^{(12,2)}_{WE} = 0.002$	$C^{(12,2)}_{WE} = 0.01$
$\phi^{(2)}_{WE}$	$C^{(2)}_{WE} = 0.005$	$C^{(2)}_{WE} = 0.06$
$\phi^{(1)}_{TI}$	$C^{(1)}_{TI} = 0.1$, $We_{c,TI1} = 6.5$	$C^{(1)}_{TI} = 0.05$, $We_{c,TI1} = 1.2$
$\phi^{(2,1)}_{TI,1}$	$C^{(2)}_{TI} = 0.02$, $We_{c,TI2} = 7.0$	$C^{(2,1)}_{TI} = 0.04$, $We_{c,TI2} = 1.2$
$\phi^{(2)}_{TI,2}$	$C^{(2)}_{TI} = 0.02$, $We_{c,TI2} = 7.0$	$C^{(2)}_{TI} = 0.01$, $We_{c,TI2} = 1.2$
$\phi^{(2,12)}_{SO,1}$	$C_{SO} = 3.8 \times 10^{-5}$	$C_{SO} = 2.5 \times 10^{-6}$
$\phi^{(2,12)}_{SO,2}$	$C_d = 4.8$, $We_{c,SO} = 4500$	$C_d = ND$, $We_{c,SO} = 4000$
$\phi^{(2)}_{SI}$	$C^{(2)}_{RC} = 0.005$, $C^{(2)}_{WE} = 0.005$	$C^{(2)}_{RC} = 0.01$, $C^{(2)}_{WE} = 0.06$

- SCHLEGEL Model (Schlegel et al., 2015)
  The work of Schlegel et al. (2015) aimed at extending the range of validity of SMITH terms by using a larger database in the tuning process. They proposed new values for some coefficients along with a modification of a few terms. The new coefficients are built on flows in pipes from 0.152 m to 0.304 m diameter, with

Table 3
Summary of coefficients and constants revised by SCHLEGEL.

Constant	SMITH coefficients	SCHLEGEL coefficients
$C_{RC}^{(12,2)}$	0.01	0.05
$C_{WE}^{(12,2)}$	0.01	0.02
$C_{WE}^{(2)}$	0.06	0.05
$C_{TI}^{(12,2)}$	0.04	0.02
$We_{c,SO}$	4000	10
C_{SO}	2.5×10^{-6}	5×10^{-5}

gas velocities of up to nearly 11 m/s and liquid velocities of up to 2 m/s, as well as conditions with both bubbly flow and cap-bubbly flow injection. The authors found that SMITH terms had prediction errors in excess of 20% for most flow conditions of the database. But, the revised IATE was able to predict interfacial area concentration and void fraction within 15% RMS error. The modified constants are given in Table 3. The most significant change is the value of $We_{c,SO}$ which is four-hundred-time less.

- Proposed model: SMITH-SUN
  A new set of Coalescence/Break-up terms have been proposed and studied in this paper. This set of terms consists of SMITH terms in which SUN coefficients replace SMITH coefficients. The choice to combine the two models stems from empirical considerations on the sets of sink/source terms for both groups of bubbles relying on an extended numerical campaign followed by systematic experimental validation.
  The first test case allowing highlighting the limitations of the models presented before was the TOPFLOW test case (see Section 4.1), which consists of an in vertical large diameter pipe. At first, the three original models, SUN, SMITH and SCHLEGER, were used to reproduce a churn regime. None of them was able to reproduce it. We realized that some coalescence and break-up terms became excessively large and could not yield a stable solution. Remember that the difference between SCHLEGER and SMITH consists in the value of some coefficients. Both were modelled against a database obtained on wide cylinders. Thus theoretically they are the most appropriate to reproduce the TOPFLOW test case. Instead, the SUN model differs from the SMITH not only in the value of some coefficients but also in the modelling of some source/sink terms. We remember that this C/B model was proposed and validated in confined rectangular section.
  Therefore, the second step was to perform a parametric study by modifying some values of the coefficients of the SUN and SMITH models (SCHELEGER is the same model of SMITH, so modifying one automatically means modifying the other) to perform a sensitivity analysis:

  – Observing the original coefficients of SMITH and SUN, each coefficient of SMITH is of the same order of magnitude as its counterpart in SUN coefficients. Most coefficients are two times higher in Random Collision (RC) terms and five times higher in Wake Entrainment (WE) terms. The critical Weber number is five times less important in the turbulent impact (TI) terms. Thus, this TI mechanism activates for smaller Weber numbers compared to SUN terms, since it activates when the Weber number exceeds the critical value, producing smaller bubbles than SUN terms. These differences led us to believe that using the SUN coefficients in the SMITH model could improve its performance in reproducing a churn regime.
    Some coefficients of SMITH's model, such as the Weak-Entrainment and the Turbulent Impact, were changed with the coefficients of the SUN model. This change permitted to reproduce the TOPFLOW test case and the results are shown in Section 4.1.1.
  – Although coefficients were modified, the SUN model was never able to obtain a satisfactory behaviour.

  This second step, allowed us to understand that in terms of modelling, the SUN model probably is not capable of reproducing all the physics that was, on the other hand, considered in SMITH and that allows such types of experimental configurations to be reproduced. From a coefficient point of view, SMITH's (and SCHLEGER's) original coefficients were not able to reproduce the chosen configuration and/or regime, except after being partly modified. Instead, SUN coefficients seemed to better activate some essential mechanisms of bubble formation and interaction.
  We therefore chose to pair the two models and test it on the TOPFLOW. The new model, SMITH-SUN, showed good agreement with the experimental data (see Section 4.1).
  Then the next step was to test the four models on the configuration for which the SUN model was developed: the confined rectangular sections (see Section 4.2). This test case allowed us to show that the SCHLEGER model is the one that shows the largest errors compared to the experimental data and compared to the other three models. Looking at coefficients that differentiate it from SMITH (see Table 3) and from SUN (see Table 2) we concluded that the chosen values do not favour the activation of certain mechanisms, as explained earlier. In particular, WE is ten times smaller than the other models. This supports the choice of preferring the coefficients of SUN. Again, the SMITH-SUN model showed good agreement with the experimental.
  Finally, to ensure that the SMITH-SUN model can reproduce the same regimes as the original model, we have reproduced also a bubbly regime in the LIU & BANKOFF configuration (see Section 4.3). Again, the SMITH-SUN showed good results and good agreement with the experimental.
  In conclusion, the SMITH-SUN model was validated on different experimental setups and three different regimes, showing in all cases a numerical error that did not exceed the 15% on the quantities of interest examined.
  However, we want to emphasize that these first analyses should be complemented with future works in order to extend the range of validity. We also want to emphasize that no calibration was performed. Surely this could be a future perspective for improving the model.

3. Numerical scheme

The NEPTUNE_CFD code is a Finite Volume Eulerian generalized multi-field solver. The numerical algorithm is based on a fractional step non-linear method that ensures conservation of mass and energy and allows strong interface source terms coupling and compressibility (variation of densities in function of pressure and enthalpy during a time step). The discretization follows a 3D full unstructured finite volume approach, with a collocated arrangement of all variables. Numerical consistency and precision for diffusive and advective fluxes for non-orthogonal and irregular cells are taken into account through a gradient reconstruction technique. Convective schemes for all variables, except pressure, are centred/upwind scheme. Velocities components can be computed with a full centred scheme. Gradients are calculated at second order for regular cells and at first order for highly irregular cells. See Mérigoux et al. (2016) for more details.

4. Results and discussion

In this section, we assess the performances of the models by simulating several configurations and regimes and comparing them with respect to experimental data. We simulate bubbly and transitional flows including cap-bubbly and churn regimes characterized by an overall void fraction less than 0.5. The validation of the IATE model and of

Table 4
Summary of the main characteristics of test cases and simulation aims.

Facility	Regime	Flow characteristics			Aim of the test case
		$\alpha_{g,max}$	Bubble diameter max. [mm]	Injection superficial velocity [m/s]	
TOPFLOW	1: churn 1	0.4	50–500	$j_g = 0.219$ $j_f = 0.405$	Validation in **large diameter pipe** (D = 195.3 mm) - Assess the limit of the C/B models
SUN	1: cap	0.3	<25	$j_g = 0.418$ $j_f = 0.631$	- Validation in confined **rectangular section** (200 × 10 mm^2) - Validation in two transitional regimes
	2: churn	0.4	<25	$j_g = 2.014$ $j_f = 2.839$	- Comparison of coal./breakup models - Source/sink mechanism analysis
LIU & BANKOFF	3: bubbly	0.25	<5	$j_g = 1.087$ $j_f = 0.027$	- Validation in **small diameter pipe** (D = 38 mm) - Validation in bubbly regime (No G2 injection)

the interaction mechanisms can be exclusively realized by an inverse procedure since no direct experimental data of coalescence/breakup phenomena are available for these experiments. However, with the exception of the SUN model, the other models have never been assessed within a CFD code, so no cross-validation of even the flow dynamics has ever been proposed. One goal of this paper is indeed to propose this kind of validation by proposing comparisons with experimental data on the evolution of gas volume fraction, phase velocity, diameters, and interfacial air.

Four test cases belonging to three experiments are proposed in the following. The main characteristics and the objectives of each test-case are given in Table 4. As explained in Section 2.3.2 (see, in particular, the SMITH-SUN model subsection) we reproduced the TOPFLOW experiment in Section 4.1 with a test case representing a churn flow in a large diameter pipe. Our goal is to assess the fours model in the churn regime. This test allows us to assess the limits of the coalescence/breakup (C/B) models. Secondly, the experiment of SUN in Section 4.2 for which two test cases in cap and churn regimes are studied. Our aim is to assess the model in a confined section and to compare predictions obtained with different coalescence and breakup models. Finally, the experiment of LIU and BANKOFF in Section 4.3 features one test case representing a bubbly flow in a small diameter pipe. Our aim is to validate the SMITH-SUN model in this regime. No bubbles of the second group are injected in this case.

Finally, remember that the Neptune_CFD code is based on the assumption that the gas and liquid phases are in pressure equilibrium. This assumption, unfortunately, defines the system as conditionally ill-posed. Thus in some areas of the domain, it may lose hyperbolicity and show unphysical oscillations. Under such conditions, mesh convergence can be impossible to achieve.

For this reason, for all tests, we nevertheless systematically performed a mesh convergence study for two reasons:

(1) to find a numerical solution potentially converging to the asymptotic solution of the numerical system we are solving,
(2) and to ensure–as much as possible–that unphysical oscillations do not appear.

4.1. TOPFLOW experiment

In this study, our goal is to assess the performance of the four models in predicting a churn regime in vertical large diameter pipe.

The measurements were carried out at the Transient twO-Phase FLOW test facility (TOPFLOW) of the Institute of Safety Research at the Forschungszentrum Dresden–Rossendorf. The facility is described in detail by Schaffrath et al. (2001) and Prasser et al. (2006). The database was built in 2007 and published by Beyer et al. (2008) and Lucas et al. (2010).

The experimental facility is pictured on Fig. 2. The test section consists of a vertical steel pipe with an inner diameter of 195.3 mm and a length of about 8 m. It is equipped with six gas injection units (see Fig. 2-c) which allow to inject air in the pipe wall. The measurement plane is situated at the upper end of the test section. A wire-mesh sensor with two measuring planes was used. For the purpose of computational efficiency, the flow was assumed to be axisymmetric. As a consequence, numerical simulations were performed on a small radial sector of the pipe with symmetry boundary conditions at both vertical sides. The geometry is a sector of 0.1 rad in the azimuthal direction and is 5.5 m long. We used a mesh with 20×1100 for obtaining a $\Delta R \approx \Delta z \approx 5$ mm. Both water and air are injected at the bottom of the test section. Data are monitored at three locations along z-axis: $z/D = 7.9, 13.3, 23.2$. The boundary conditions used are summarized in Table 5. Calculations are performed during 50 s. All quantities of interest are time-averaged from the twentieth second.

4.1.1. Comparison SMITH and SMITH-SUN coalescence/breakup models

As this experiment is in a large diameter pipe, SMITH model is expected to allow a better overall prediction.

However, the results obtained with this coalescence/breakup terms were not satisfactory. Similarly, the SUN and SCHLEGER models failed to provide a solution on this case. Focusing on the SMITH model, the main discrepancy was observed on the Group-2 interfacial area concentration and diameter which can be attributed to a failure in coalescence/breakup models. Dominant mechanisms for this large diameter configuration are wake entrainment and turbulent impact. A parametric study has been done in order to identify which coefficients in SMITH terms play a major role in the current configuration and can explain the deterioration observed in the results. A modification of some coefficients was found necessary to correctly predict the behaviour of large bubbles. Some SMITH coefficients have been replaced by SUN coefficients. For the wake entrainment process, the coefficient $C_{WE}^{(2)}$ was reduced from 0.06 to 0.005. For the turbulent impact process, the critical Weber numbers $We_{c,TI1}$ and $We_{c,TI2}$ were raised from 1.2 to 7.0 and the coefficient $C_{TI}^{(2,1)}$ was reduced from 0.04 to 0.02. All other coefficients were kept unchanged. These modifications mitigate the contributions of the wake entrainment mechanism by 100% and the turbulent impact mechanism by more than 50%. We then performed the same simulations with SMITH-SUN terms. These simulations were found in good agreement with experimental data. Fig. 3 shows the IAC and total void fraction with modified SMITH model and SMITH-SUN model. The two models show the same behaviour.

Table 5
Boundary conditions used for TOPFLOW simulations.

TOPFLOW	α_{g1}	α_{g2}	D_{sm1} (mm)	D_{sm2} (mm)	v_{g1} (m/s)	v_{g2} (m/s)	v_l (m/s)
Churn test case	0.1	0.25	6	15	0.8	0.8	0.8

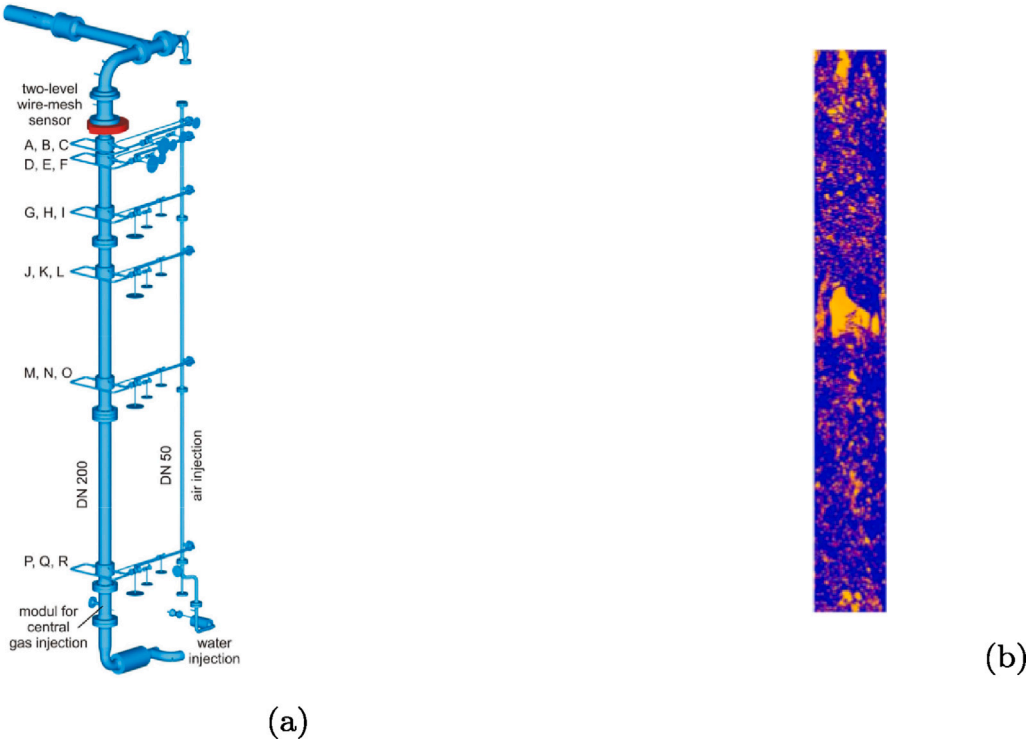

Fig. 2. (a) TOPFLOW test section; (b) virtual sectional of the void distribution for the churn test case.

4.1.2. Calculations with SMITH-SUN terms

We propose here the analysis and validation of the SMITH-SUN modelon on this test case. Figs. 4(a–b) show the interfacial area concentration and the void fraction, respectively. In abscissa, the radial position with the centre of the channel at position 0. Numerical predictions are in good agreement with experiment on all three levels. There are almost no huge differences with the height, in fact we can observe almost the same experimental curves. The same behaviour is observed also in the numerical curves (see Fig. 4) and in the volume fraction contour in Fig. 6.

Figs. 4(c–d) show the gas fraction of each gas field individually. A wall-peaking behaviour is observable for smaller bubbles (G-1 bubbles). This behaviour is attributed to the fact that the centre of the channel is occupied by large bubbles. Indeed, the larger bubbles are present, the more small bubbles are pushed near the wall (see Figs. 5(e–f)).

Moreover, we observe that this behaviour in Group-1 void fraction is not always kept as well as the radial distribution of Group-2 void fraction. The Sauter mean diameter for Group-1 bubbles is uniform around 6 mm along the radial position except close to the wall where a sharp decrease is noticeable. For Group-2 bubbles, the diameter varies between 12 mm and 20 mm and the predictions are in good agreement with an under-prediction of 10%. Probably the decrease observed for G-1 is due to the error made with respect to the velocity profile near the wall (see Fig. 5). The change in velocity with height is negligible and no clear increase or decrease can be identified. Quantitatively, the experimental data and the numerical predictions are in good agreement. The maximum error is around 10%. However, in some cases, the concavity of the numerical predictions do not comply with that of experimental data.

4.2. SUN Experiment (Sun et al., 2004a)

The experimental data collected by Sun et al. (2004a) are used to perform our study. The experimental facility includes a two-phase mixing section, a rectangular test section, an upper plenum, a water reservoir, water and air delivery systems and instrumentation. The cross sectional dimensions of the test section are 200 mm in width (in x) and 10 mm in gap (in y). The total height of the test section is around 3 m (in z). The hydraulic diameter is $D_h = 19.05$ mm. An adiabatic air–water mixture flow upward through the test section at room temperature. The loop is operated under atmospheric pressure. Experiments with different flow conditions in cap-turbulent and churn-turbulent flow regimes are carried out. The acquired local quantities of interest are the time-averaged void fraction, the interfacial velocity, the bubble number frequency, the interfacial area concentration, and the bubble Sauter mean diameter for each group of bubbles. Moreover the Sun's experience provides measurements for both groups of bubbles. so besides being one interesting test for the comparison of interaction mechanisms, this experience represents an excellent test case for the validation of the two-group IATE model. These data are line-averaged over y direction. Measurement port are located at $z/D = 35$, 88 and 142.

The computational geometry consists of a quarter of the real test section with cross dimensions 100 mm in width (in x) and 5 mm in gap (in y) and of 2700 mm high (in z). The inlet section of the computational domain is located at the first measurement port of the test section and the outlet is located almost $35D$ after the last measurement point (see Fig. 7).

In this work, the measurement data at the first measurement port ($z/D = 35$) are used to specify inlet boundary conditions, as in Lee et al. (2013). The outlet boundary condition is a pressure outlet at the

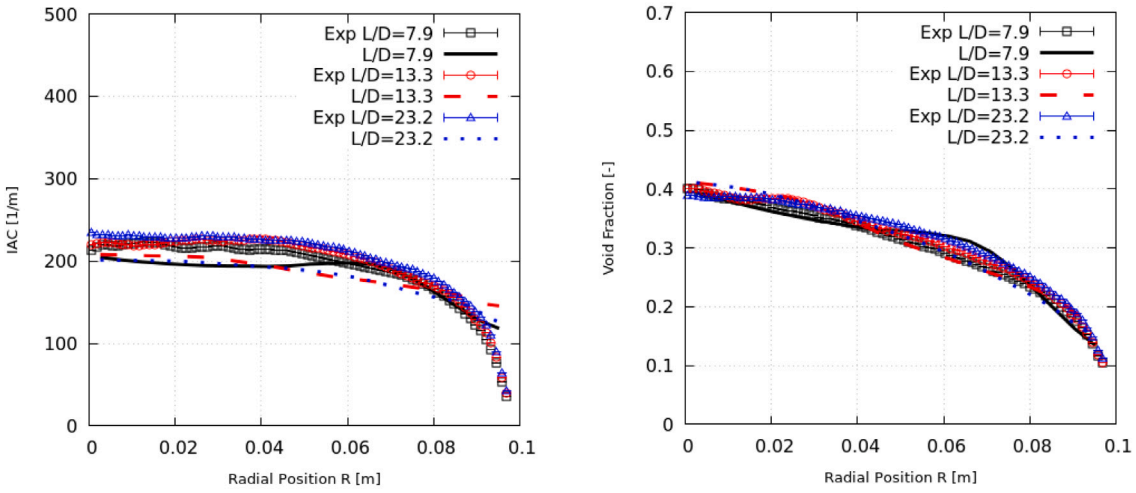

(a) Modified SMITH model: IAC

(b) Modified SMITH model: total α_g

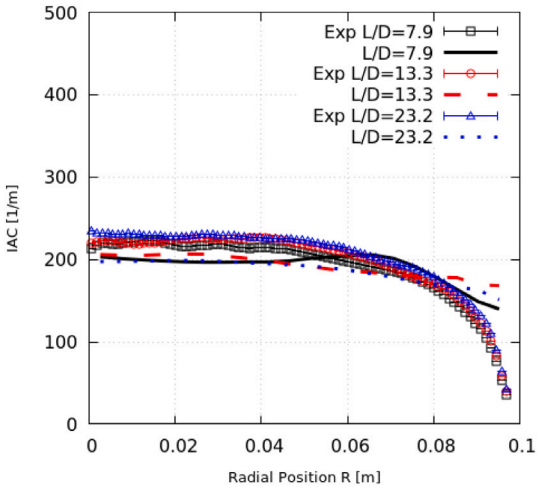

(c) SMITH-SUN model: IAC

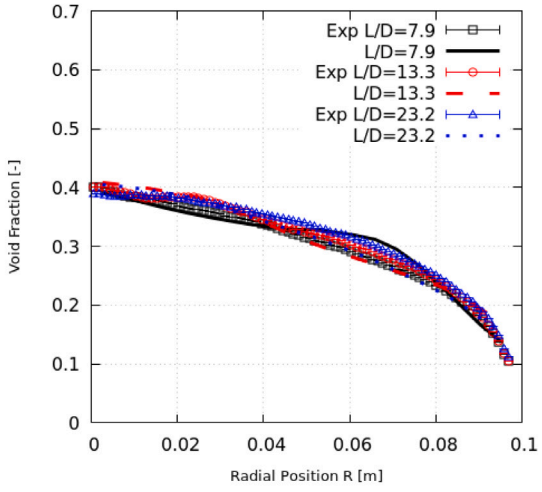

(d) SMITH-SUN model: total void fraction

Fig. 3. Comparison of Interfacial area concentration (IAC) and total void fraction calculated with SMITH modified and SMITH-SUN coalescence and breakup models for case Churn.

atmospheric pressure. On the two external lateral boundaries a wall condition is applied while a symmetry condition is applied on the two internal lateral boundary. Two test cases were simulated and showed in the following: RUN 13 (Cap-bubbly flow) and RUN 14 (Churn-turbulent flow) (see Sun et al., 2004a).

4.2.1. Mesh sensitivity analysis

A mesh sensitivity analysis was done in the cap-bubbly test case, using the new SMITH-SUN model. Concerning the test conditions, the inlet void fractions for Group-1 and Group-2 bubbles are 33.3% and 1.2% respectively. The inlet bubble diameters for Group-1 and Group-2 bubbles are 3.16 mm and 17.4 mm. At the inlet position, the superficial gas velocity is $j_g = 0.418$ m/s and the superficial liquid velocity is $j_f = 0.631$ m/s. We remember that superficial flow velocity is the hypothetical velocity calculated as if the given phase were the only one flowing in the inlet sectional area. The critical diameter, D_c, is equal to 11 mm. Hexahedral meshes are used. A sensitivity analysis has been performed on the three meshes reported in Table 6. We remember that the computational domain consists of 200 mm in width (in x), 10 mm in gap (in y) and 2700 mm high (in z). So, considering large size of the experimental apparatus, the three meshes were obtained considering uniform refinement. The turbulence model used in all simulations (SSG model Mérigoux et al., 2016) imposes a law on the first mesh: it was not necessary to refine close to the wall.

Table 6
Mesh characteristics. (Δx (mm), Δy (mm), Δz (mm)).

Mesh 1	$25 \times 8 \times 400$	$\Delta x = 4,\ \Delta y = 0.63,\ \Delta z = 6.75$
Mesh 2	$50 \times 16 \times 550$	$\Delta x = 2,\ \Delta y = 0.31,\ \Delta z = 4.91$
Mesh 3	$75 \times 24 \times 650$	$\Delta x = 1.33,\ \Delta y = 0.21,\ \Delta z = 4.15$

In Fig. 8, we compare the three meshes with respect to the interfacial area concentration, the void fraction, the Sauter mean diameter and the gas velocity at the height $z/D = 88$. For ease of reading, the mesh sensitivity analysis at $Z/D = 142$ (Fig. D.23) is available in Appendix D.1.

Analysing the interfacial area concentration, the void fraction, the Sauter mean diameter and the gas velocity, the relative errors between the results obtained with Mesh 2 and Mesh 1 remain less than 1% except for the gas velocity in the wall region where the relative error between Mesh 2 and Mesh 1 raises to 24%. The relative error of the results with Mesh 2 and Mesh 3 remains less than 1% except for the interfacial area concentration of Group-1 bubbles for which the relative error raises to 4%.

Using Meshes 2 and 3, convergence was already achieved, so there was no need to refine further and Mesh 2 is used for all the following simulations.

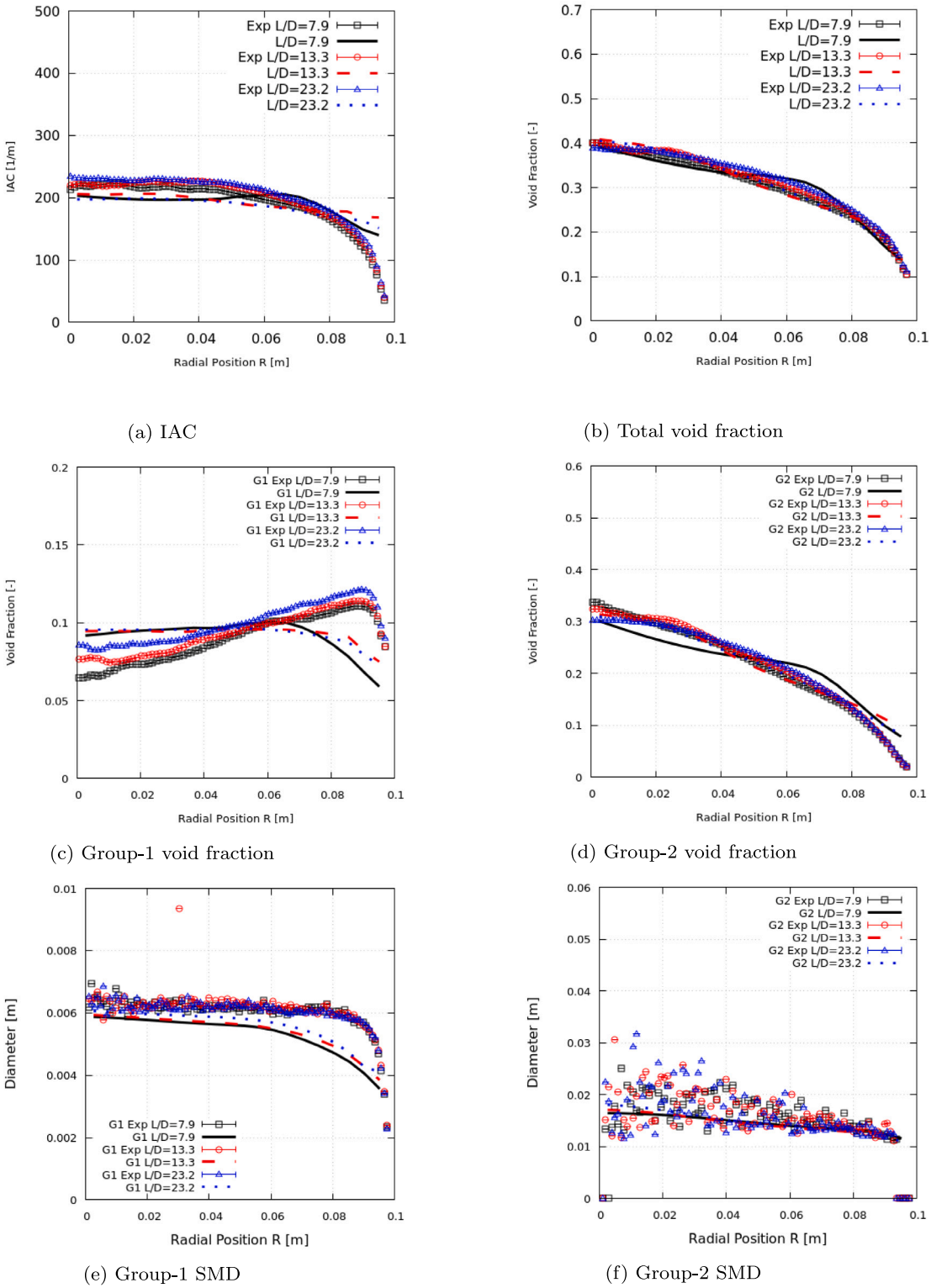

(a) IAC

(b) Total void fraction

(c) Group-1 void fraction

(d) Group-2 void fraction

(e) Group-1 SMD

(f) Group-2 SMD

Fig. 4. Comparison between the experimental data TOPFLOW and the numerical solution obtained by SMITH-SUN model.

4.2.2. Cap-bubbly flow

Simulations of the aforementioned cap-bubbly regime have been made with four different sets of source/sink terms for the two-group interfacial area transport equations: SUN terms, SMITH terms, SCHLEGEL terms and SMITH-SUN terms. We recall that SUN terms have been developed with the current geometry, while SMITH and SCHLEGEL terms have been established to target flows in large diameter pipes. Some comparisons between the results at the two heights $z/D = 88$ and $z/D = 142$ are presented hereafter.

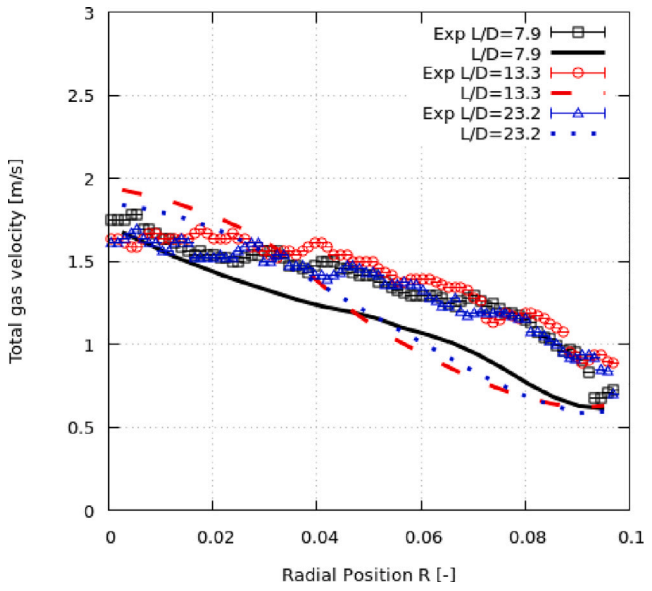

Fig. 5. Comparison between the experimental total gas velocity TOPFLOW and the numerical solution obtained by SMITH-SUN model.

- ***Comparisons at z/D = 88***

  In Fig. 9, comparisons of the experimental data with experimental error bars and the results obtained from simulations with the four source terms are presented.

Concerning Group-1 bubbles, the IAC is over-predicted by 12% by the model with SUN and SCHLEGEL terms while a good agreement is found with SMITH and SMITH-SUN terms (see Fig. 9, black lines). Qualitatively, the trend of the four curves complies with that of measured data, showing a good prediction of the experimental wall peak distribution. The predicted values of void fraction and Sauter diameter are almost equal with the four source/sink terms, and they perfectly meet the experimental data, including close to the wall.

The predicted velocity for Group-1 bubbles is similar with the four sets of terms. It is also in good agreement with experimental data in the centre region while an over-prediction by 5% near the wall is observed.

Concerning Group-2 bubbles, their amount is minimal for this case. Nevertheless, the Sauter mean diameter is under-predicted by the four models (see Fig. 9, red lines). The profiles are flat in the middle region and decrease near the wall ($(x = 0\,\mathrm{m})$). Results with SUN and SMITH-SUN terms are better with an error of 30%. For SCHLEGEL terms, the error raises to 50%. Moreover, the Sauter mean diameter predicted with SCHLEGEL terms near the wall is below the critical diameter equal to 11 mm, which is not physically and numerically acceptable.

There is an over-prediction of 40% (between $x = 0.04$ mm and $x = 0.15$) of the velocity results with the four models compared to the experimental data. Computed results show that Group-2 bubbles, which are larger than Group-1 bubbles, also travel at a higher speed. This is coherent with the buoyancy force. We note that a similar result has been found in Lee et al. (2013) too.

However, according to the experimental data, bubbles are larger than the predictions but move very close to that of Group-1

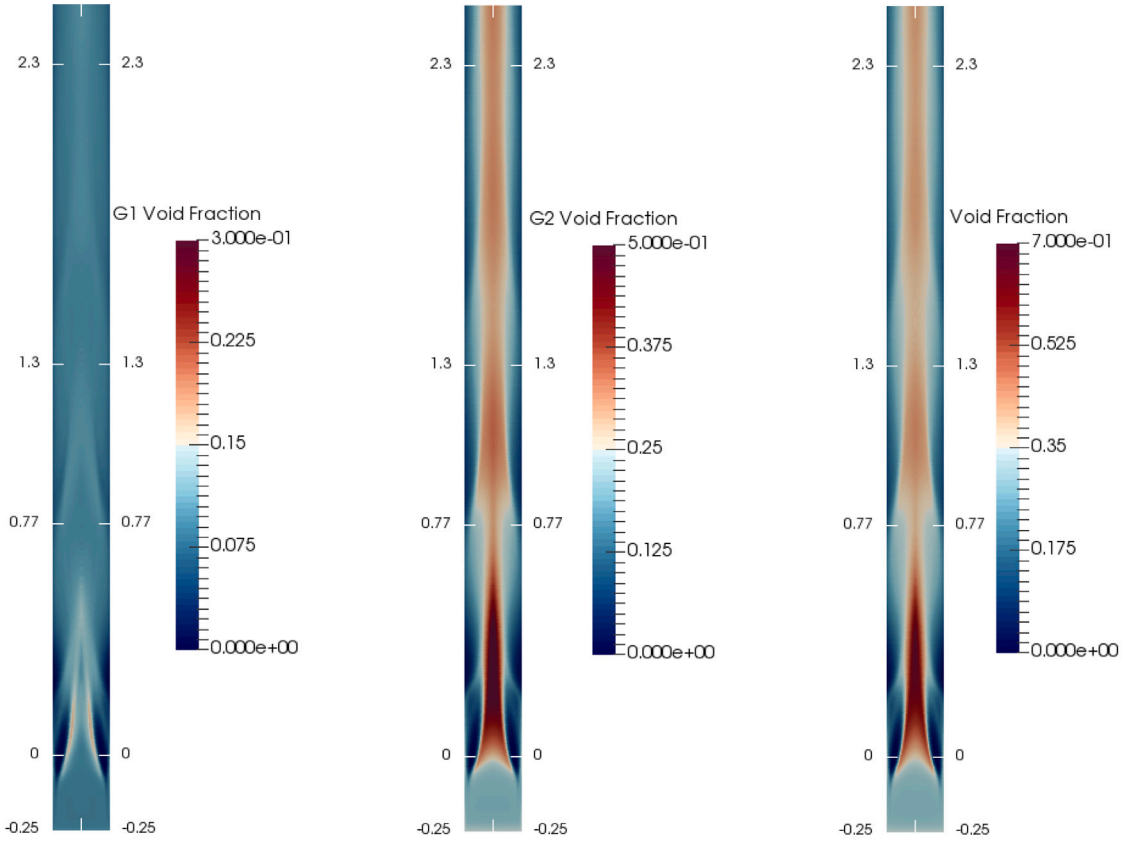

(a) G1 Void Fraction (b) G2 Void Fraction (c) Total Void Fraction

Fig. 6. Contours of the void fraction for case Churn in TOPFLOW experiment.

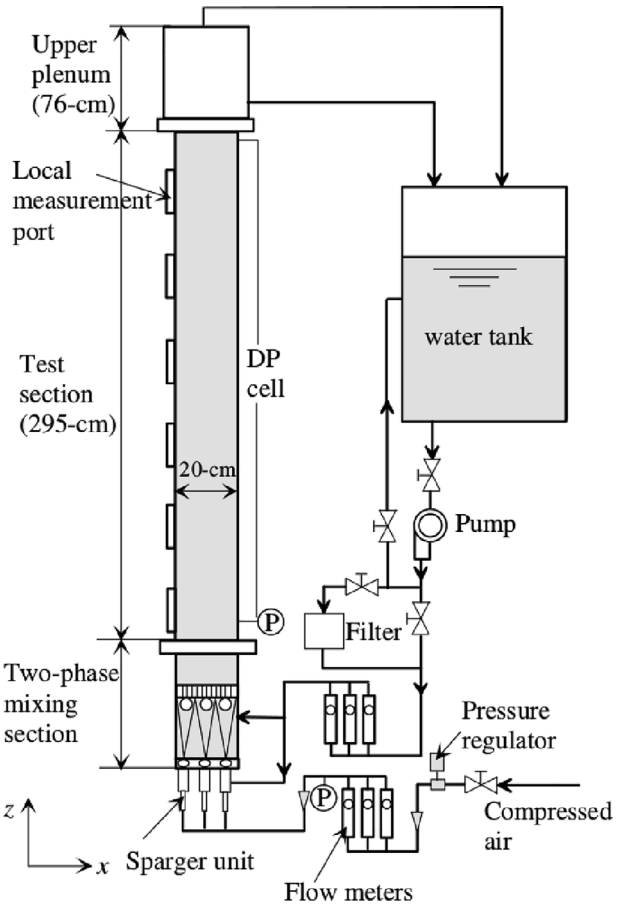

Fig. 7. SUN experiment: schematic of the experimental loop.
Source: From Sun et al. (2004a).

bubbles in the centre region and at a smaller velocity near the wall. This behaviour is in contradiction to what we expect in an infinite liquid domain. The confined dimension in the y-direction probably works to reduce the travelling velocity of Group-2 bubbles. The discrepancies observed for Group-2 bubbles may reflect the difficulty of making accurate measurements due to the low frequency of Group-2 bubbles encountering the probe sensors compared to Group-1 bubbles for this flow condition. Moreover, concerning the velocity variable, the interfacial velocity is measured and not the gas transport velocity. It has already been reported (Schlegel et al., 2014) that these velocities are similar for small bubbles belonging to Group-1 but could be pretty different for cap and churn bubbles belonging to Group-2. This behaviour is because Group-2 bubbles are more deformable due to hydrodynamic forces.

The validation step shown in Fig. 9 allows us to identify which model generates the lowest error for the four examined quantities. Now the analysis turns to the interaction terms to understand which mechanisms could generate this error. So in Figs. 10 and 11, we can observe and compare the trend of the interaction mechanisms for the four models in the Group 1 and 2, respectively.

Concerning Group 1, the comparison in Fig. 10 between SUN and SMITH shows that the Turbulent Impact (TI) mechanism is more important for SUN. This mechanism is a breakup process that forms smaller bubbles. Its higher positive contribution with SUN terms for Group-1 bubbles leads to an increase in the IAC. On the contrary, the Random Collision (RC) mechanism is less important for SMITH than SUN terms. The random collision mechanism is a coalescence process that forms larger bubbles. Its higher negative contribution with SUN causes a decrease in the interfacial area concentration. The effect of the turbulent impact is dominant over random collision leading to a higher positive contribution with SUN than with SMITH. This difference could explain why the interfacial area concentration is higher for SUN terms than for SMITH terms.

SCHLEGEL terms are similar to SMITH terms except for the shearing-off (SO) mechanism raised by more than two orders of magnitude. Group-1 bubbles are created from this mechanism, causing an increase in the IAC. Regarding SMITH-SUN terms, the contributions of random collision and turbulent impact, which are the main mechanisms with SUN terms and SMITH, are mitigated. To summarize, the IAC predicted with SUN terms is higher because of a higher contribution of the turbulent impact mechanism, while the IAC predicted with SCHLEGEL terms is higher because of an increase of the shearing-off mechanism. Fig. 11 shows the y-line-averaged source/sink terms for Group-2 bubbles. The wake entertainment contribution is dominant in SUN, SMITH and, mainly, in SCHLEGEL. This term is a coalescence mechanism that usually decreases the IAC and increases the diameter, but, in this case, its positive value produces an inverse effect, decreasing the diameter (as we can show in Fig. 9). The shearing-off process plays a relatively significant contribution in the SCHLEGEL model since it increases the diameter reduction. The sum of these two effects explains the differences between SUN (or SMITH-SUN) and SCHLEGEL in terms of diameter.

Finally, we can summarize that the SMITH-SUN model shows a better behaviour than the other models, even if, except for SCHLEGEL, SUN and SMITH models show similar results than SMITH-SUN. Concerning the source/sink terms, three mechanisms should be improved or modified for a better and global performance enhancement: the Turbulent Impact and the Shearing-off for Group-1 and the Wake Entrainement for Group-2.

- ***Comparisons at $z/D = 142$***

We propose in this sub-section the same analysis as proposed for z/D = 88, but at a higher height ($z/D = 142$) in order to analyse the axial evolution of the flow (see Fig. 12).

Concerning Group-1 bubbles, we can conclude similar observations than the previous height for the four models. In other words, SCHLEGEL and SUN overestimate the IAC (with a maximum error equal to 26% and 20% for SUN and SCHLEGEL, respectively); instead, SMITH and SMITH-SUN follow the same trend of experimental points, always staying in the upper limit of the error experimental bars. The four models show the same behaviour concerning the gas volume fraction and the Sauter diameter. All models estimate correctly the gas velocity.

Concerning Group-2 bubbles, the IAC is highly over-predicted with SCHLEGEL, and the bubble diameter drops dramatically under the critical diameter. The significant over-prediction of the IAC is not due to a greater volume of Group-2 bubbles, but this mainly comes from substantial contributions of breakup sink terms causing an excessive breakup of Group-2 bubbles. Consequently, the bubble diameters decrease below the critical diameter, becoming a non-physical value.

With SMITH terms, a significant drop in the diameter is also observable compared to the previous position. The relative error reaches 20%. With SUN and SMITH-SUN terms, the diameter is well above the critical diameter and is under-predicted with a maximum error of 10% at $x = 0.4$. We note that at this height ($z/D = 142$), the error on Sauter's diameter estimate is smaller than that observed at $z/D = 88$. So, we can conclude that the SMITH-SUN model shows a good agreement with the

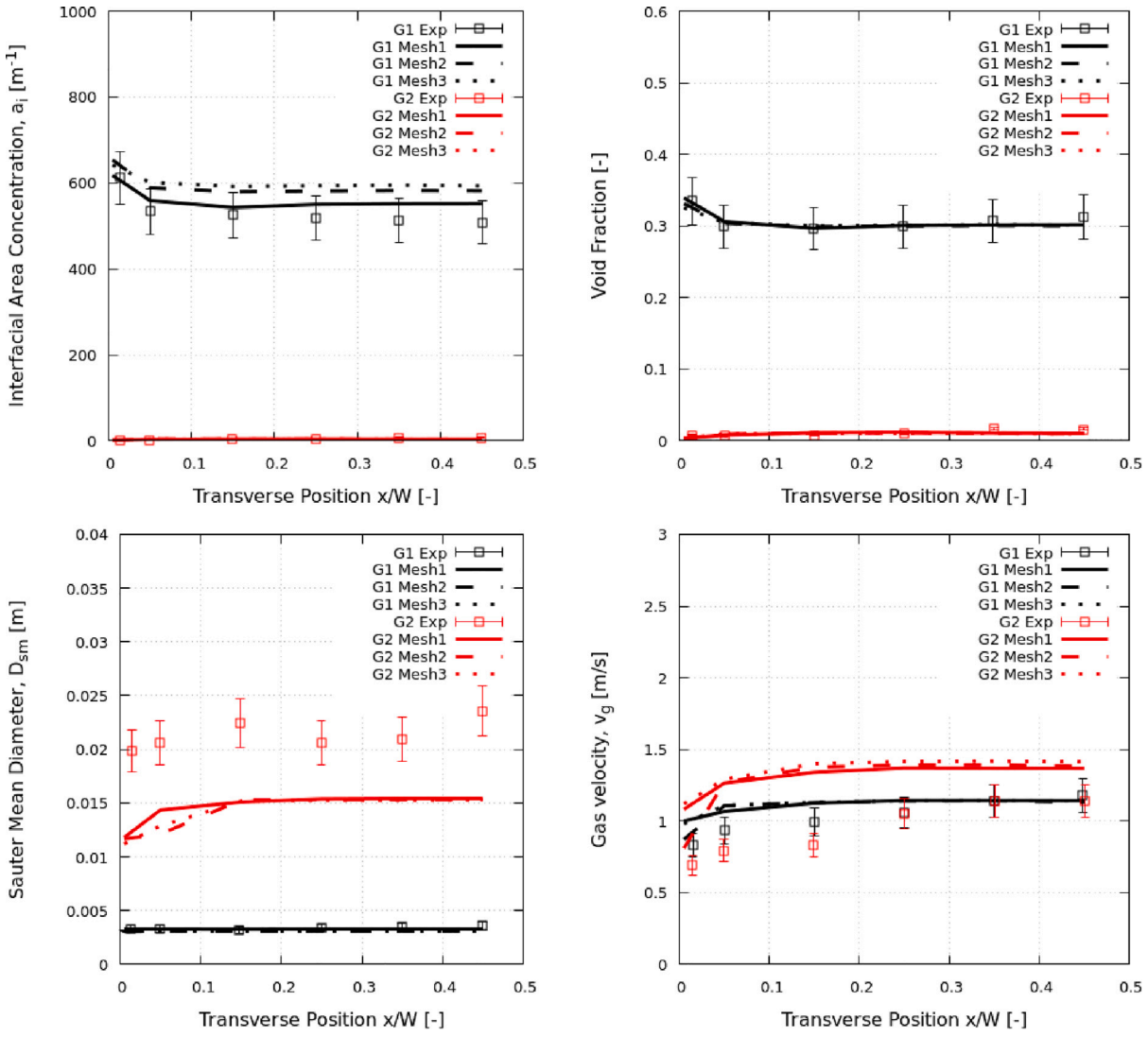

Fig. 8. Cap-bubbly: benchmark between the three meshes and experimental data at z/D = 88, using the new SMITH-SUN as coalescence and breakup model.

experimental data, and it globally estimates all variables better than the other models.

We try now to identify the source/sink terms that are responsible for the differences between the four models. So, focusing on the source/sink terms (see Figs. 13 for Group-1 and 14 for Group-2), we find similar results than the previous height.

Concerning Group-1, as at $z/D = 88$, the dominant mechanism in the SUN model is the *Turbulent Impact*, much larger than in the other models, and that it is not equilibrated by the *Random Collision*. Concerning the SCHLEGEL model, we can observe some differences with respect to $z/D = 88$, since in this case, it is the negative *Weak Entrainement* that produce the over-prediction of the IAC.

Concerning Group-2, as observed at $z/D = 88$, the *Weak-Entrainement* seems to produce the most significant differences between the SCHLEGEL and the SMITH models, with respect to the SUN and SMITH-SUN.

Finally, we can summarize that the SMITH-SUN model shows a better behaviour than the other models, even if, except SCHLEGEL, SUN and SMITH models show similar results than SMITH-SUN. Concerning the source/sink terms, two mechanisms should be improved for a better and global performance enhancement: the Turbulent Impact for Group-1 and the Wake Entrainement for Group-2.

4.2.3. *Churn-turbulent flow*

The churn-turbulent flow regime is characterized by higher inlet gas and liquid velocities ($j_g = 2.014$ m/s, $j_f = 2.839$ m/s) and by higher inlet void fractions for Group-1 and Group-2 bubbles (7.5% and 19.1% respectively) than the Cap-bubbly flow. The inlet bubble diameters for Group-1 and Group-2 bubbles are 2.87 mm and 28.84 mm. The critical diameter is equal to 11 mm. Mesh 2 is used for all the following simulations (see Section 4.2.1).

- ***Comparisons at z/D = 88***

  The plots of the IAC, the void fraction, the Sauter mean diameter and the velocity at the height $z/D = 88$ are showed in Fig. 15.

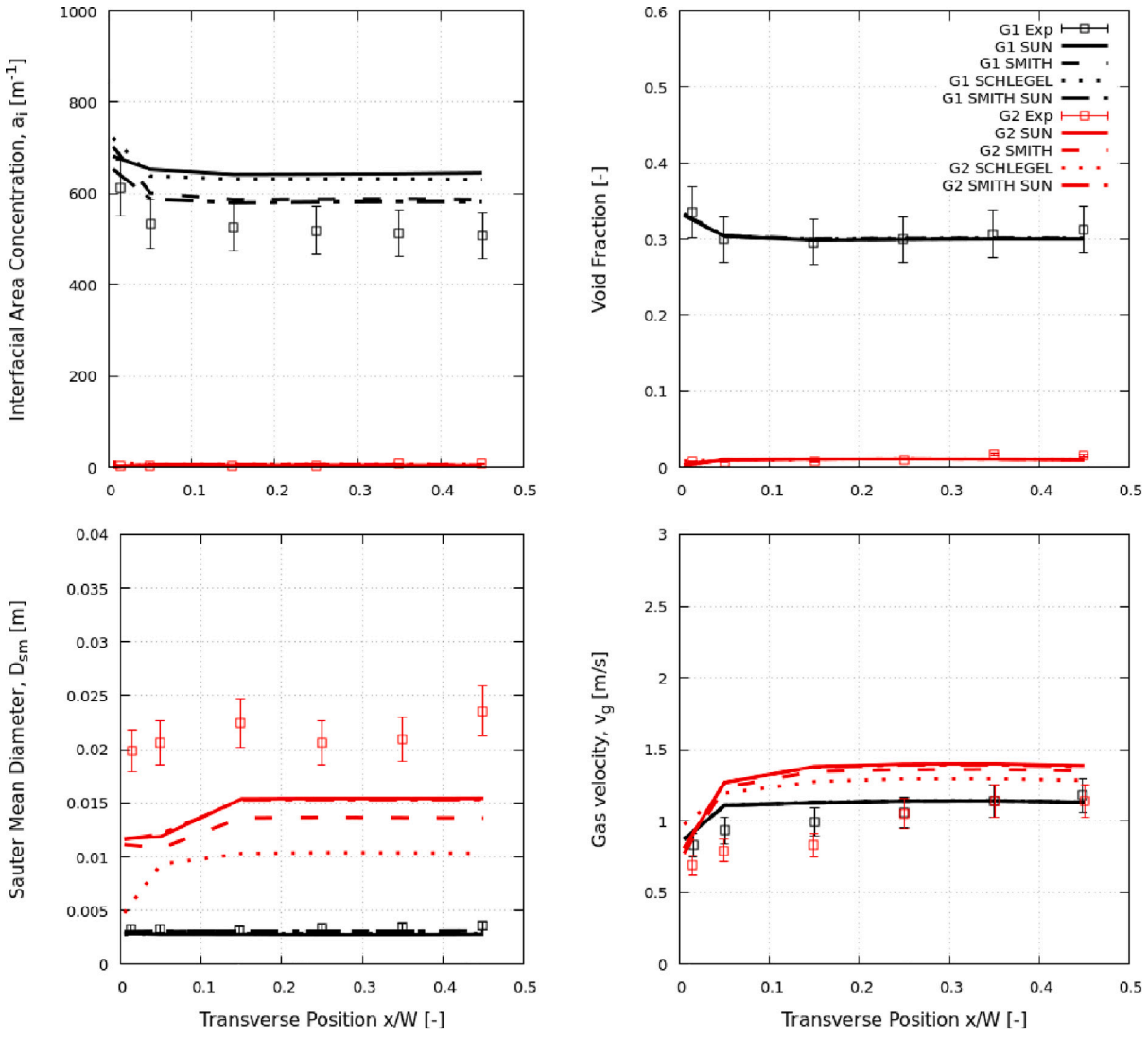

Fig. 9. Benchmark of line-averaged predicted results against experimental data at $z/D = 88$ for a cap-bubbly flow regime: interfacial area concentration, void fraction, Sauter mean diameter, gas velocity. Group-1 in black and Group-2 in red. (For interpretation of the references to colour in this figure legend, the reader is referred to the web version of this article.)

For what concerns Group-1 bubbles, compared to the experimental data, the IAC predicted with SUN, SMITH and SMITH SUN terms are close to experimental data (see Fig. 15, black lines). Close to the wall, the wall peak distribution is reproduced with a better performance with the SMITH model. With SCHLEGEL terms, the IAC is over-predicted by 10%. With the four source/sink terms, the predicted values for the void fraction are almost identical and meet the experimental data (see Fig. 15-b, black lines). The void fraction is almost uniform along the section, except for a little increase near the wall. This exception indicates that experimentally, the sharp increase in the IAC in the region near the wall is due to an accumulation of gas and smaller bubbles that allow a higher surface for the same gas volume. Concerning the Sauter mean diameter for Group-1 bubbles, the predictions with all models are close one to another and meet the experimental data (see Fig. 15 black lines). The velocity is under-predicted with a maximum error of 13% as compared to experimental data by all models.

For what concerns Group-2 bubbles, the results obtained with the four source/sink terms for the IAC, the void fraction and the gas velocity are in good agreement with the experimental data (see Fig. 15 red lines). However, the void fraction and the velocity are under-predicted by 5% and 10%, respectively, in the centre of the channel. The predicted Sauter mean Diameter is in good agreement with experimental data, even though all models, and particularly the SMITH-SUN model, under-estimate it (see Fig. 15, red lines), showing a maximum error close to the wall.

Overall, the SUN model performs very well for this test case, but SMITH performs as well. The replacement of the coefficients in SMITH terms to form SMITH-SUN terms has a limited effect on a churn-turbulent flow.

Fig. 16 shows the y-line-averaged source/sink terms for Group-1 bubbles.

Concerning the source/sink terms, the comparison between all models is given in Fig. 16 and in Fig. 17 for Group-1 and Group-2, respectively.

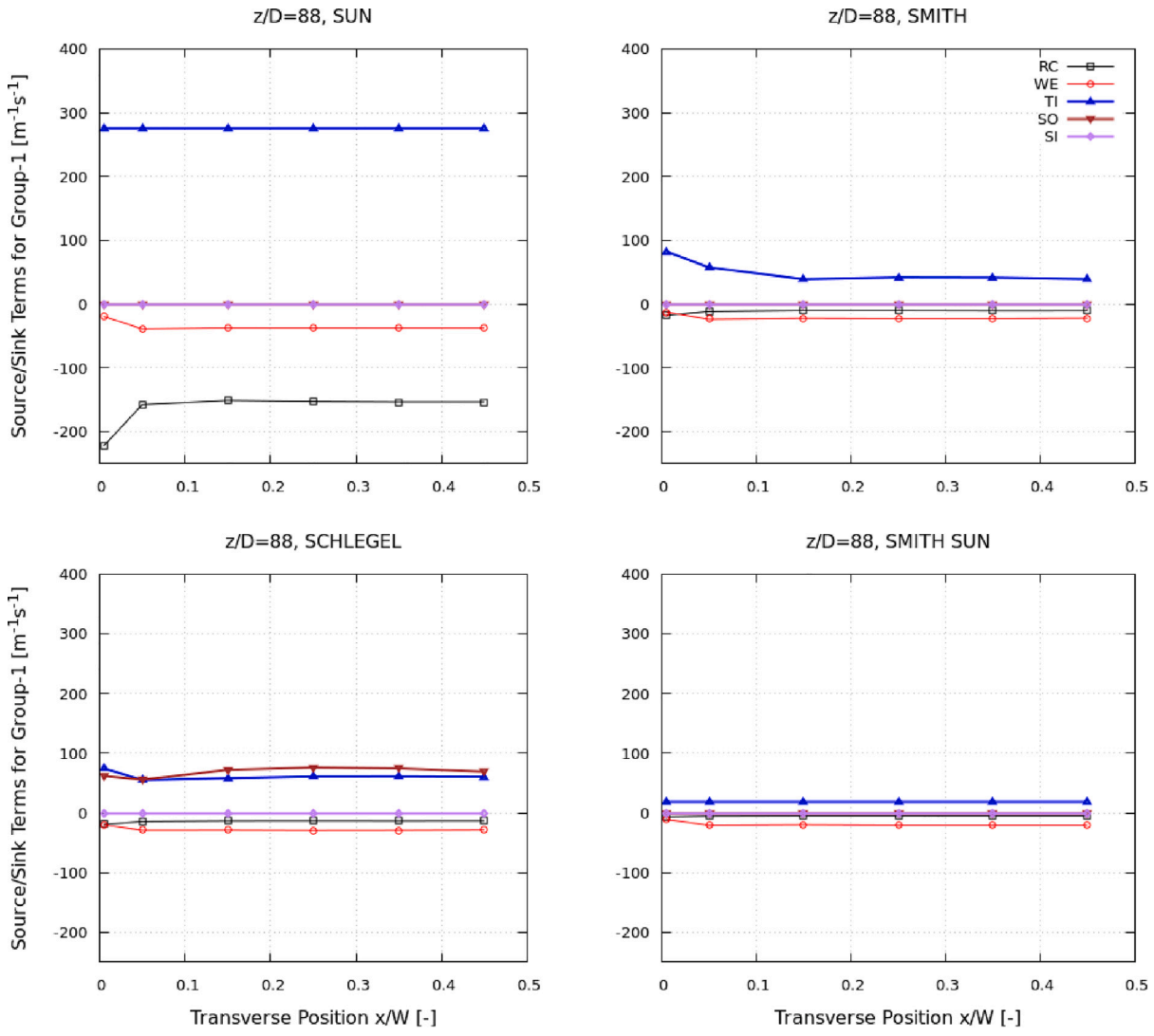

Fig. 10. Cap-bubbly flow. Comparison of line-averaged coalescence/breakup mechanisms for Group-1 bubbles for SUN, SMITH, SCHLEGEL and SMITH-SUN terms at z/D = 88.

Using SUN terms, turbulent impact and shearing-off are the main mechanisms. With SMITH terms, the only predominant mechanism is the turbulent impact. Both shearing-off and turbulent impact mechanisms are breakup mechanisms that create a smaller bubble and increase the IAC. The turbulent impact mechanism with SMITH terms increases sharply in the region near the wall. Thus, the higher IAC is due to this mechanism.

With SCHLEGEL terms, the shearing-off mechanism dominates away from the wall while the turbulent impact mechanism dominates near the wall, similarly to results with SMITH terms. The excessive shearing-off mechanism explains the important overprediction of the IAC. With SMITH-SUN terms, the turbulent mechanism remains dominant but is strongly mitigated. In comparison to the previous cap-bubbly case, the turbulent impact mechanism plays a key role in both regimes to increase the IAC by producing smaller bubbles. The shearing-off mechanism is much more significant in the churn regime than in the cap-bubbly regime with SUN and SCHLEGEL source terms. This is expected because Group-2 bubbles are larger than in the cap regime, and a greater number of them that may undergo this mechanism are encountered in the churn regime.

Concerning Group-2 bubbles, with SMITH terms as well as SCHLEGEL terms, the turbulent impact mechanism and the wake entrainment dominate. With SMITH-SUN terms, the turbulent impact mechanism is the dominant term, while the wake entrainment mechanism is mitigated as compared to SMITH terms.

Compared to the previous cap-bubbly case, the wake entertainment mechanism is crucial in both regimes. In the churn regime, its negative contribution is caused by the merging of mainly Group-2 bubbles, decreasing the IAC of Group-2 bubbles and increasing the average bubble size. In the cap-bubbly regime, the positive contribution indicates that several Group-1 bubbles undergo this mechanism to form Group-2 bubbles. The intergroup transfer from Group-1 to Group-2 bubbles explains the increase in the IAC due to this mechanism.

- ***Comparisons at z/D = 142***

  The same comparisons proposed at $z/D = 88$, have been made at a higher height.

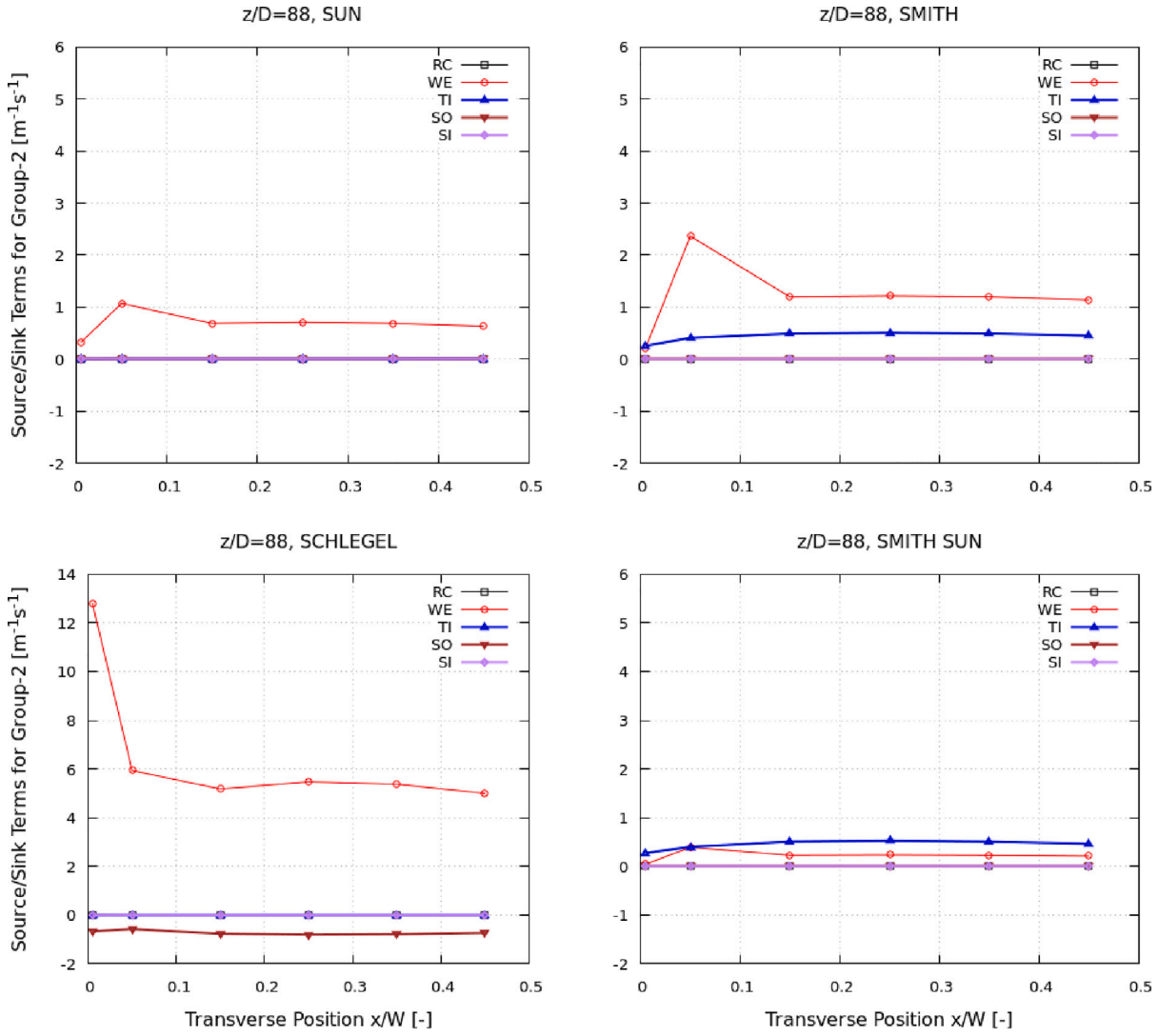

Fig. 11. Cap-bubbly flow. Comparison of line-averaged coalescence/breakup mechanisms for Group-2 bubbles for SUN, SMITH, SCHLEGEL and SMITH-SUN terms at z/D = 88.

In Fig. 18, no significant change is observed in the profiles of the four variables and with the four source/sink terms. The same trends observed at the lower height are kept here. In between the two heights, Group-2 bubbles grow a little, but the flow regime remains unchanged.

The four source/sink terms are plotted on Fig. 19 for Group-1 and on Fig. 20. The same discussion made at the lower height also applies to these results.

4.3. LIU and BANKOFF experiment

In this study, we simulate a bubbly flow configuration in a small diameter pipe. An important aspect of this test case is that in this configuration, the void fraction is less than 0.3 and the maximum bubble diameter is less than 5 mm which corresponds to a bubbly flow. As a consequence, this case allows verifying that by imposing a zero injection of bubbles of Group-2, the model is still able to well reproduce a bubbly flow without Group-2 development. This configuration has been studied experimentally by Liu and Bankoff (1993). It features an upward bubbly flow in a circular pipe. It represents a water/air two-phase flow with a low void fraction. The flow is isothermal, incompressible and turbulent with a Reynolds number equal to 47 000. The test case section is a 2800 mm long, vertical smooth acrylic tubing, with inner diameter of 38 mm. Bubbles are produced by injecting air into a bundle of 64 equally-spaced 0.1 mm needles.

4.3.1. Simulation setup and numerical details

The geometry is a circular pipe with an inner diameter of 38 mm and a height of 2800 mm. In the selected experimental test case, the bubble diameter at the injection location is equal to 1 mm. The void fraction at the inlet is 0.0176. At the inlet, the water mean axial velocity is equal to 1.106 m/s and the gas mean axial velocity is equal to 1.534 m/s.

The void fraction is very low and the bubble size is narrow. Three hexahedral meshes have been tested with 10, 20 and 40 cells in the diameter. The mesh size is respectively 3.8, 1.9 and 0.95 mm.

All gas injected belong to the first gas field and the maximum bubble size remains less than the critical diameter between the two gas fields. SMITH-SUN coalescence and breakup model has been used

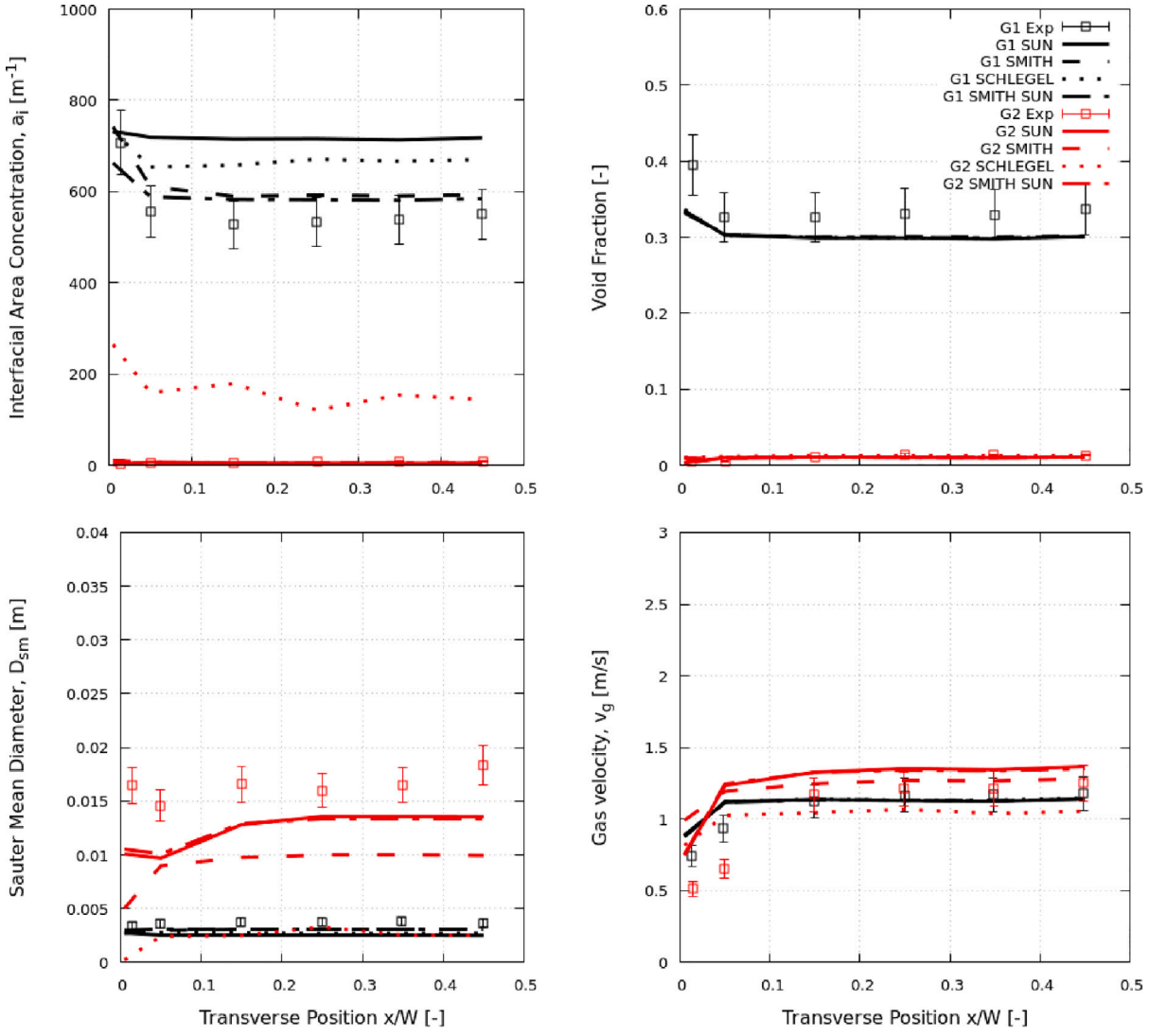

Fig. 12. Benchmark of line-averaged predicted results against experimental data at $z/D = 142$ for a cap-bubbly flow regime: interfacial area concentration, void fraction, Sauter mean diameter, gas velocity. Group-1 in black and Group-2 in red. (For interpretation of the references to colour in this figure legend, the reader is referred to the web version of this article.)

as source/sink terms in the two-group IATE model. This choice has been made because the effect of the wall is more important in small diameter pipe compared to large diameter pipe and SUN coefficients that appear in SMITH-SUN terms have been tuned in a confined test section with important wall effects.

4.3.2. Results

Fig. 21 presents comparisons for void fraction at the end of the test section. In abscissa, there is the adimensional radial coordinate. The wall is on the right side. Group-1 void fraction is plotted as no Group-2 void fraction appears during the simulation. A good prediction is obtained compared to experimental data. Most of the gas phase is pulled towards the wall thanks to the lift force. This effect is reproduced by the model.

Fig. 22 presents comparisons for liquid velocity, liquid turbulent shear stress, liquid fluctuating velocities in radial and axial directions at the end of the test section. The profile of the liquid velocity is well predicted. The relative error with respect to the experimental data remains less than 5%. The profiles of the shear-stress distribution and turbulent fluctuation quantities are also well reproduced, but an under-prediction is observable with our model by up to 20%. However, experimental errors on measurements are not available for a comparison with the discrepancies.

5. Conclusion

The objective of this work is to assess the performance of several sets of source/sink terms appearing in the two-group Interfacial Area Transport Equation model, specifically in 3D simulations of complex bubbly, cap-bubbly and churn regimes exhibiting bubbles of different shapes and with broad bubble size distribution. Coupled with a three-field model, the two-group Interfacial Area Transport Equation model allows handling the polydispersity of bubbles in transitional regimes, including cap-bubbly and churn-turbulent regime. These flows are characterized by a broad bubble size distribution with the presence of

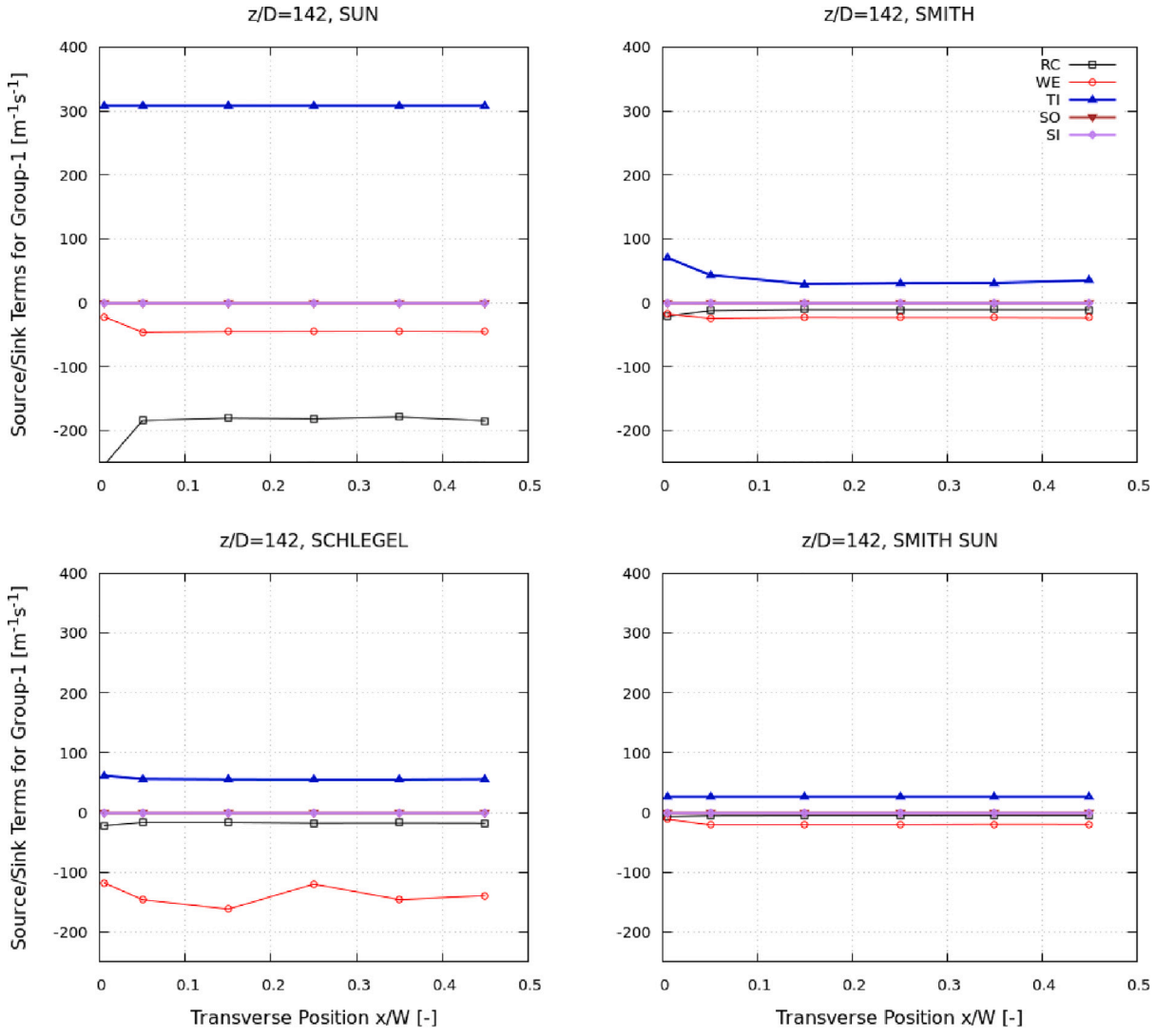

Fig. 13. Cap-bubbly flow. Comparison of line-averaged coalescence/breakup mechanisms for Group-1 bubbles for SUN, SMITH, SCHLEGEL and SMITH-SUN terms at z/D = 142.

bubbles with various shapes: spherical, distorted, cap and churn bubbles. Bubbles are classified into Group-1 bubbles (spherical, distorted) and Group-2 bubbles (cap, churn) and the change in the interfacial area concentration of each bubble group is dynamically tracked by means of two transport equations. Bubble interactions are accounted for as source/sink terms, and five mechanisms are modelled: random collision and wake entrainment, turbulent impact, shearing-off and surface instability.

The first contribution of this paper is then to investigate and compare several bubble interaction mechanisms of coalescence and fragmentation for the 2-Group Interfacial Area Transport Equation (IATE) model. For two of these models, this is the first time their performances are assessed within a CFD code. Specifically, three different sets of terms are compared together: SUN terms originally designed for flows in confined rectangular sections, SMITH and SCHLEGEL terms originally developed for flows in large diameter pipes. A fourth set of terms combining SUN and SMITH terms, called SMITH-SUN in this paper, has been proposed here, which constitutes the second contribution of this work. Finally, a validation versus experimental data has been performed on three experiments and four test cases allowing the validation on three regimes : bubbly, cap-bubbly and a churn-turbulent flow conditions.

In NEPTUNE_CFD code, a three-field model whose fields are liquid, Group-1 bubbles and Group-2 bubbles are implemented. Drag, lift, turbulent dispersion, added mass forces are considered in the simulations.

Some major conclusions can be drawn from the numerical campaign:

- For large diameters (TOPFLOW experiment), the original SUN, SMITH and SCHLEGER models were unable to determine an acceptable solution for the examined churn regime. Exclusively, the SMITH-SUN model has been able to reproduce this regime. Exclusively for the SMITH model, a combination of new coefficients was found to yield an acceptable solution. The latter was compared with that obtained through the new SMITH-SUN model. Both showed good agreement with respect to the experimental values of gas volume fraction. Exclusively for the SMITH-SUN model, the analysis has been shown in terms of total gas phase

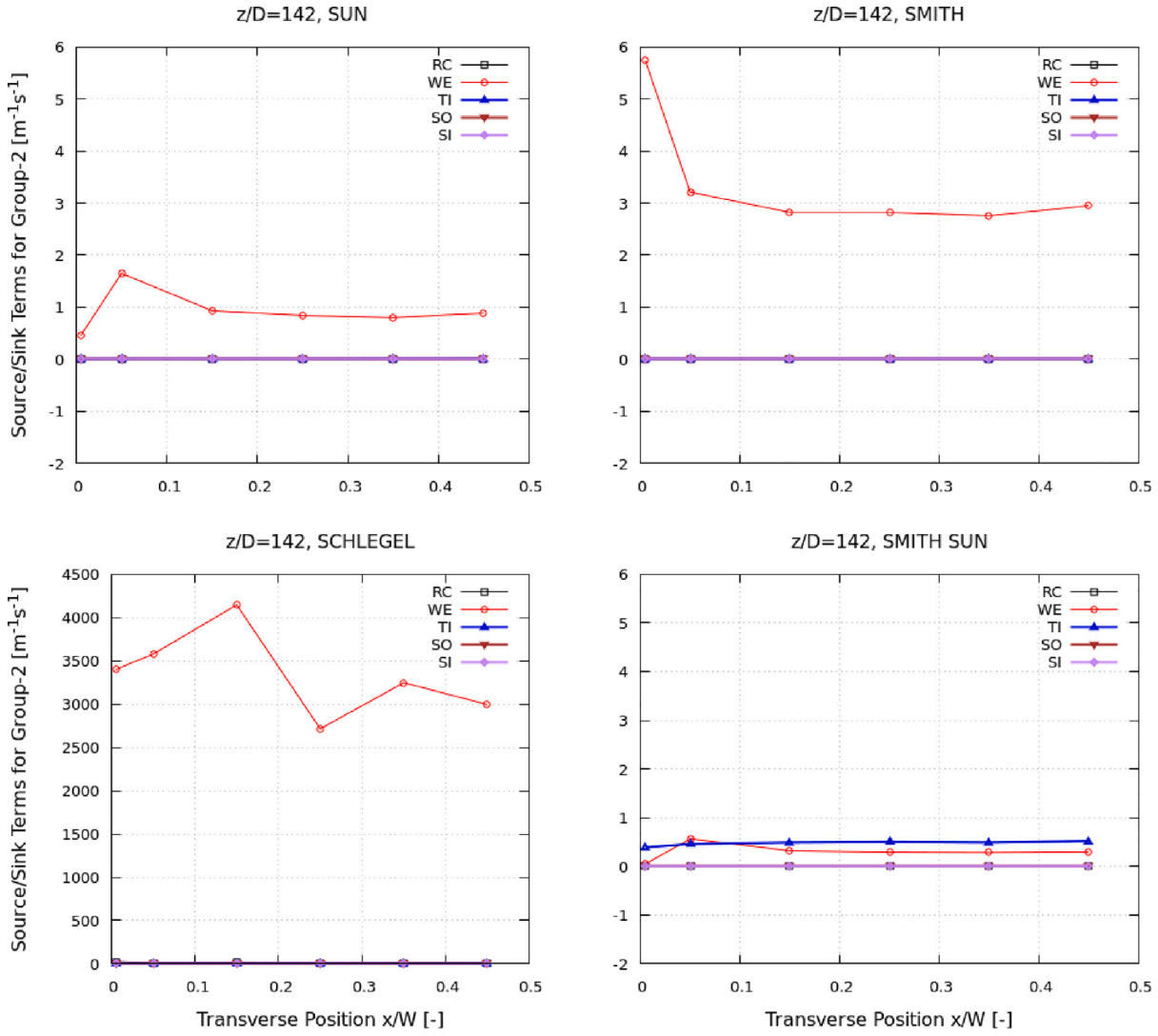

Fig. 14. Cap-bubbly flow. Comparison of line-averaged coalescence/breakup mechanisms for Group-2 bubbles for SUN, SMITH, SCHLEGEL and SMITH-SUN terms at z/D = 142.

velocity and gas volume fraction and Sauter diameter for each group of bubbles.

- Regarding the confined rectangular section configurations (SUN experiment), all four models were able to reproduce the two chosen regimes : cap and churn. SUN terms that are tailor-made for this experiment performs well but not significantly better than SMITH terms. Computations made with SCHLEGEL terms clearly showed an over-prediction of the shearing-off mechanism mainly due to the parameter $We_{c,SO}$ whose value is four hundred times lower than SUN or SMITH terms. With SMITH-SUN terms, dominant interaction mechanisms are mitigated. The results of computations with these terms remain close to that of SMITH and SUN terms.

  Finally, three mechanisms were observed to come into play in both cap and churn regimes: Turbulent impact (TI), Shearing-Off (SO) and Wake Entrainment (WE). We observed, in particular, that for all examined positions, the best model (or the best models) showed a good trade-off between the TI and the SO for the Group-1 bubbles and TI and WE for the Group-2 bubbles. In the cap-bubbly test case, the Random Collision for the Group-1 bubble and some models showed a weird behaviour, but probably to balance the TI effect.
- The SMITH-SUN model was also tested in a bubbly regime (LIU-BANKOFF experiment), showing, like the original SMITH model, the ability to reproduce this type of configuration.

Future works will be devoted to including additional configurations and regimes during the validation study. A calibration from experimental data will also be systematically targeted to take advantage of the Uncertainty Quantification methodology to compare experimental and numerical solutions more rigorously.

Declaration of competing interest

The authors declare that they have no known competing financial interests or personal relationships that could have appeared to influence the work reported in this paper.

Data availability

Data will be made available on request.

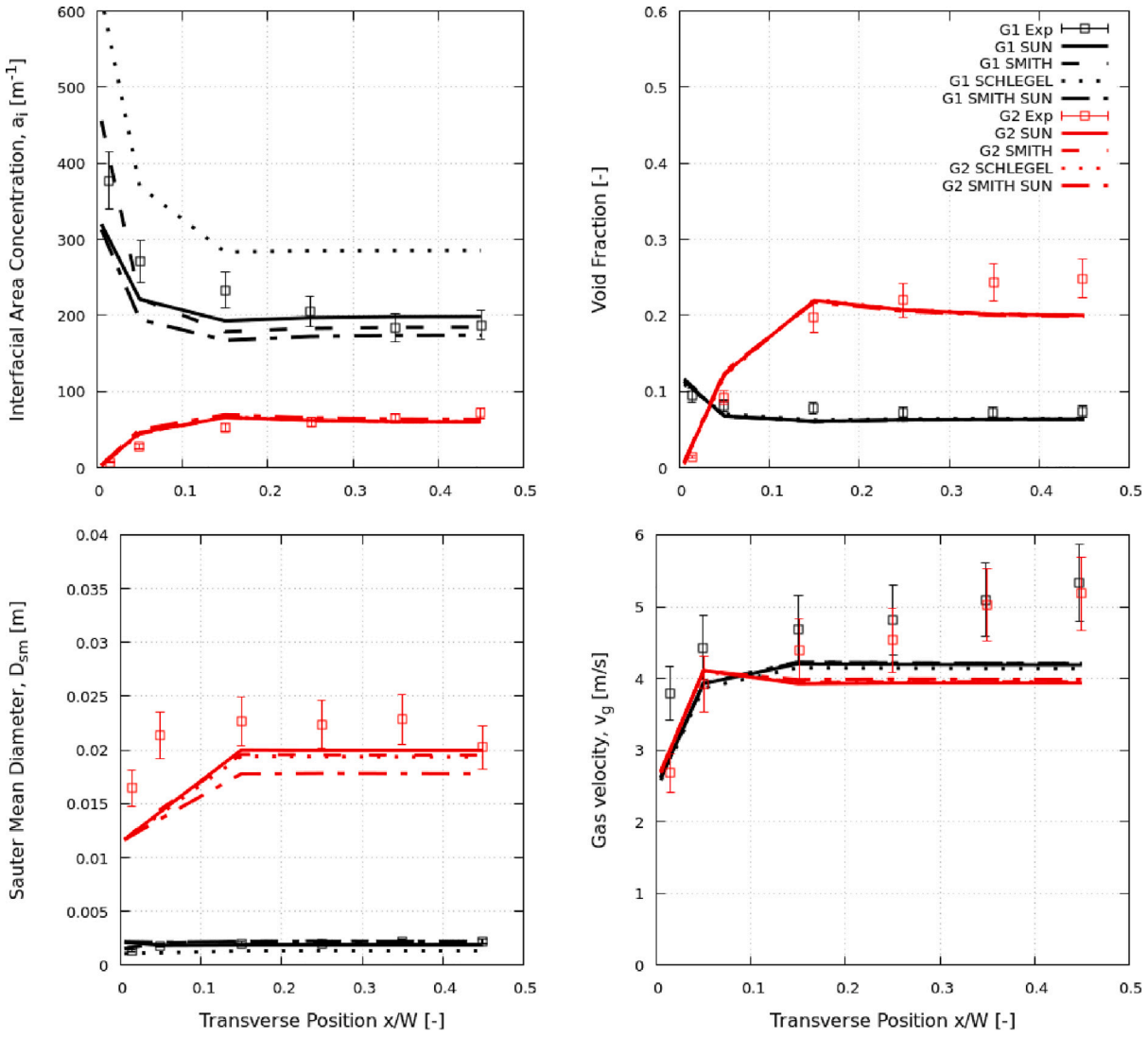

Fig. 15. Benchmark of line-averaged predicted results against experimental data at $z/D = 88$ for a churn-turbulent flow regime: interfacial area concentration, void fraction, Sauter mean diameter, gas velocity. Group-1 in black and Group-2 in red. (For interpretation of the references to colour in this figure legend, the reader is referred to the web version of this article.)

Appendix A. Interfacial forces

The expression of each force will now be given. For the sake of brevity, only the major information are given:

- Drag force
  The drag force is the force exerted in the flow direction against the bubble movement. According to Ishii and Zuber (1979), the drag force is expressed as:

$$\mathbf{M}^D_{l\to gk} = -\frac{1}{8} a_{ik}\rho_l C_{Dk}(\mathbf{v}_{gk} - \mathbf{v}_l)|\mathbf{v}_{gk} - \mathbf{v}_l| \tag{A.1}$$

  where a_{ik} is the interfacial area concentration and C_{Dk} is the drag coefficient:

$$C_{Dk} = \frac{2}{3} D_{smk}\sqrt{\frac{g|\rho_g - \rho_l|}{\sigma}}\left(\frac{1 + 17.67(f(\alpha_{gk}))^{6/7}}{18.67 f(\alpha_{gk})}\right) \tag{A.2}$$

  where $f(\alpha_{gk}) = (1 - \alpha_{gk})^{3/2}$.
- Lift force
  Unlike the drag force, the lift force acts in the transverse direction. This force is given by

$$\mathbf{M}^L_{l\to gk} = -C_{Lk}\alpha_{gk}\rho_l(\mathbf{V}_{gk} - \mathbf{V}_l)\times(\nabla\times\mathbf{V}_l) \qquad k = 1, 2 \tag{A.3}$$

where C_{Lk} is the lift coefficient for bubbles of Group−k. Tomiyama et al. (2002) expressed the lift force depending on a modified Eötvös number as follows:

$$C_{Lk} = \begin{cases} \min[0.288\tanh(0.121 Re_{,k}), f(Eo_{H,k})] & \text{if } Eo_{H,k} < 4 \\ f(Eo_{H,k}) & \text{if } 4 \le Eo_{H,k} \le 10 \\ -0.29 & \text{if } Eo_{H,k} > 10 \end{cases} \tag{A.4}$$

where

$$f(Eo_{H,k}) = 0.00105 Eo^3_{H,k} - 0.0159 Eo^2_{H,k} - 0.0204 Eo_{H,k} + 0.474 \tag{A.5}$$

where the modified Eötvös number $Eo_{H,k}$ is defined as:

$$Eo_{H,k} = \frac{g(\rho_l - \rho_g)D^2_{H,k}}{\sigma} \tag{A.6}$$

where $D_{H,k}$ is the maximum horizontal dimension of the deformed bubble, which is calculated by using an empirical correlation given by Wellek Gürkan and Wellek (1976):

$$D_{H,k} = D_{b,k}(1 + 0.163 Eo^{0.757}_{,k})^{1/3} \tag{A.7}$$

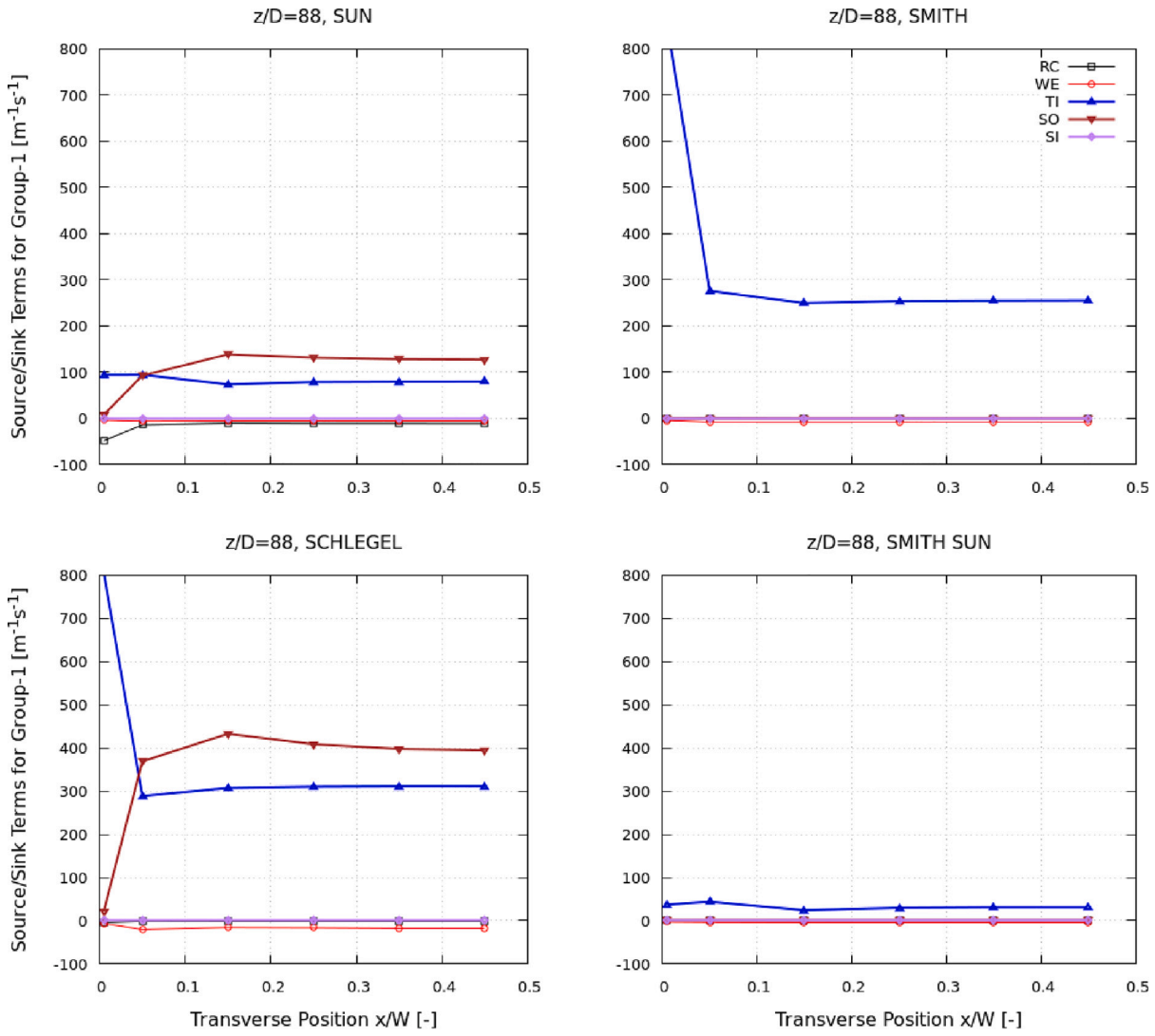

Fig. 16. Churn-turbulent flow. Comparison of line-averaged coalescence/breakup mechanisms for Group-1 bubbles for SUN, SMITH, SCHLEGEL and SMITH-SUN terms at z/D = 88.

where $D_{b,k}$ is the volume equivalent bubble diameter and the Eötvös number $Eo_{,k}$ is

$$Eo_{,k} = \frac{g(\rho_l - \rho_g)D_{b,k}^2}{\sigma} \tag{A.8}$$

For each group of bubbles, the volume equivalent bubble diameter $D_{b,k}$ is taken equal to the Sauter mean diameter D_{smk}. (In the previous equations, $k = 1, 2$). This lift coefficient allows positive and negative values depending on the bubble size. In a pipe flow for example, this will lead to wall peaking for small bubbles and core peaking for bigger ones.

- Turbulent dispersion force

The turbulent dispersion force plays a role in the lateral distribution of the gas phase. It mainly results in dispersion of bubbles from high to low volume fraction regions due to liquid turbulent fluctuations (Laviéville et al., 2017). This contribution is supposed to balance the lift and drag effect in radial direction of the flow. In this study, the Generalized Turbulent Dispersion Model (GTD) (Laviéville et al., 2017) is used. A formal derivation of this force as well as comparison to other classical formulations of the turbulent dispersion force (Lopez De Bertodano, 1998; Burns et al., 2004) can be found in Laviéville et al. (2017). The turbulent dispersion force is written as

$$\mathbf{M}_{l\to gk}^{TD} = -GTD_k\, \rho_l k_l \nabla \alpha_{gk} \tag{A.9}$$

with:

$$GTD_k = \left(\langle F_D \rangle \tau_{lg_k}^t - 1\right) \frac{b + \eta_r}{1 + \eta_r} + \langle C_{AM} \rangle \frac{b^2 + \eta_r}{1 + \eta_r} \tag{A.10}$$

$$\eta_r = \frac{\tau_{lg_k}^t}{\tau_{lg_k}^F}, \quad b = \frac{\rho_l + \rho_l C_{AM}}{\rho_{gk} + \rho_l C_{AM}} \tag{A.11}$$

$$\tau_{lg_k}^t = \frac{3}{2} C_\mu \frac{k_l}{\epsilon_l} \left(1 + \beta \frac{V_r^2}{k_l}\right)^{-1/2}, \quad \beta = 2.7, \quad \tau_{lg_k}^F = \frac{1}{F_D}\left(\frac{\rho_{gk}}{\rho_l} + C_{AM}\right) \tag{A.12}$$

C_{AM} is the added mass coefficient equal to $\frac{1}{2}$.

- Added mass force

The added mass force occurs when bubbles accelerate relative to the liquid. The inertia of the liquid mass encountered by the bubbles exerts a force on the particles. The added mass force is expressed as:

$$\mathbf{M}_{l\to gk}^{AM} = -C_{AM}\alpha_{gk}\frac{1 + 2\alpha_{gk}}{1 - \alpha_{gk}}\rho_l \left[\left(\frac{\partial \mathbf{V}_{gk}}{\partial t} + \mathbf{V}_{gk}.\nabla \mathbf{V}_{gk}\right) - \left(\frac{\partial \mathbf{V}_l}{\partial t} + \mathbf{V}_l.\nabla \mathbf{V}_l\right)\right] \tag{A.13}$$

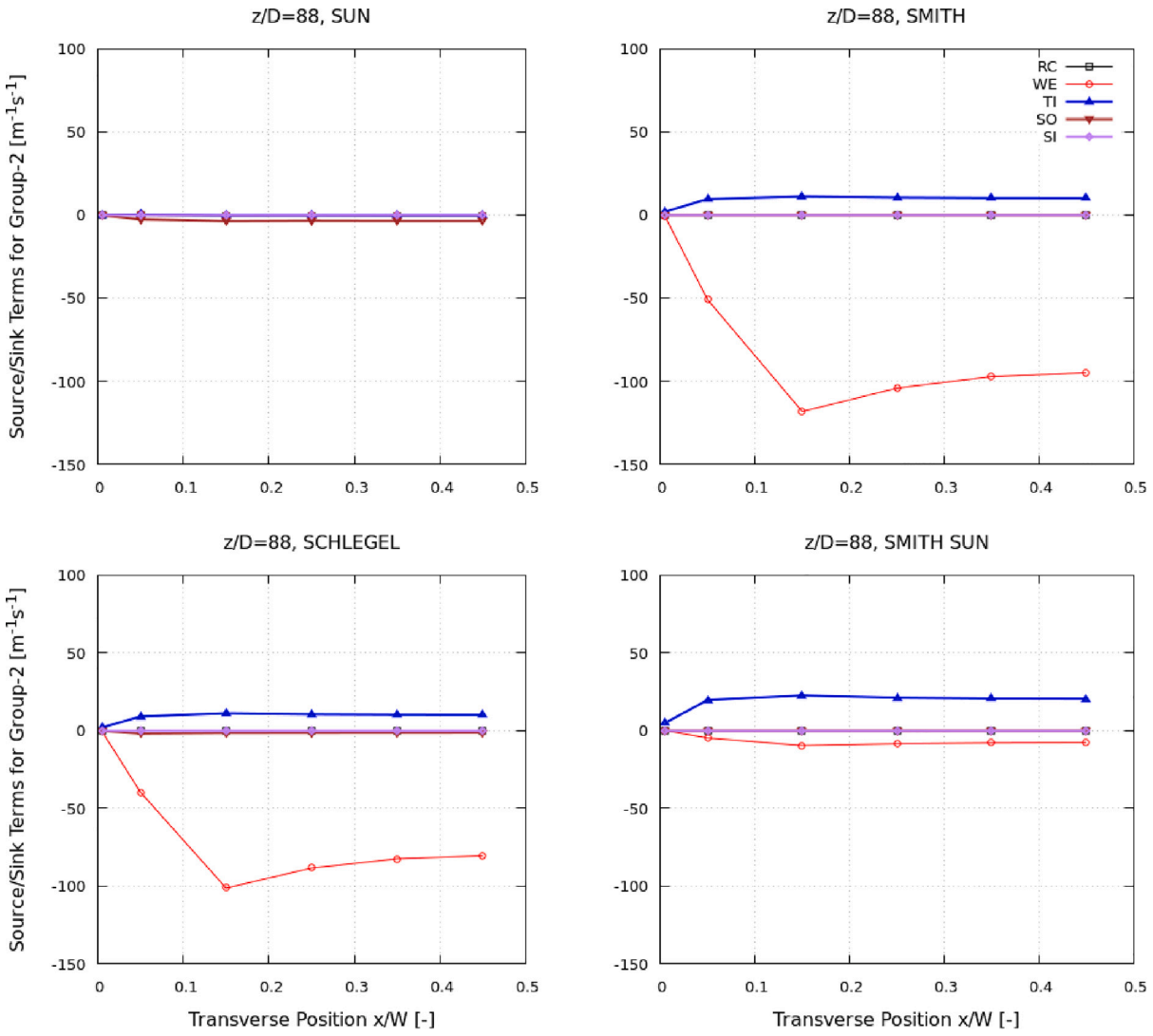

Fig. 17. Churn-turbulent flow. Comparison of line-averaged coalescence/breakup mechanisms for Group-2 bubbles for SUN, SMITH, SCHLEGEL and SMITH-SUN terms at z/D = 88.

where C_{AM} is the added mass coefficient equal to $\frac{1}{2}$ and the factor $(1+2\alpha_{gk})/(1-\alpha_{gk})$ takes into account the effect of the bubbles concentration (Zuber, 1964).

Appendix B. Coalescence/breakup terms proposed by Sun et al. (2004c)

- Random Collision RC

The source/sink terms modelling the Random Collision (RC) process are:

$$\phi_{RC}^{(1)} = -0.17 C_{RC}^{(1)} \frac{\varepsilon^{1/3}\alpha_{g1}a_{i1}^{5/3}}{\alpha_{g1,max}^{1/3}\left(\alpha_{g1,max}^{1/3}-\alpha_{g1}^{1/3}\right)} \times \left[1-\exp\left(-C_{RC1}\frac{\alpha_{g1,max}^{1/3}\alpha_{g1}^{1/3}}{\alpha_{g1,max}^{1/3}-\alpha_{g1}^{1/3}}\right)\right] \tag{B.1}$$

$$\phi_{RC,2}^{(11,2)} = 0.68 C_{RC}^{(1)} \frac{\varepsilon^{1/3}\alpha_{g1}^{2}a_{i1}^{2/3}}{\alpha_{g1,max}^{2/3}G}\left[1-\exp\left(-C_{RC1}\frac{\alpha_{g1,max}^{1/3}\alpha_{g1}^{1/3}}{\alpha_{g1,max}^{1/3}-\alpha_{g1}^{1/3}}\right)\right] \times \left(1-\frac{2}{3}D_{c1}^{*}\right) \tag{B.2}$$

$$\times \left[1+0.7G^{7/6}\left(\frac{a_{i1}}{\alpha_1}\right)^{1/2}\left(\frac{\sigma}{g\Delta\rho}\right)^{-1/3}\right] \tag{B.3}$$

$$\phi_{RC,1}^{(12,2)} = -4.85 C_{RC}^{(12,2)}\varepsilon^{1/3}\alpha_{g1}^{2/3}\alpha_{g2}^{2}\frac{a_{i1}}{R_{m2}^{2/3}} \times \left[1-\exp\left(-C_{RC1}\frac{\alpha_{g1,max}^{1/3}\alpha_{g1}^{1/3}}{\alpha_{g1,max}^{1/3}-\alpha_{g1}^{1/3}}\right)\right] \tag{B.4}$$

$$\phi_{RC,2}^{(12,2)} = 13.6 C_{RC}^{(12,2)}\varepsilon^{1/3}\frac{\alpha_{g1}^{5/3}\alpha_{g2}^{2}}{R_{m2}^{2/3}G}\left[1-\exp\left(-C_{RC1}\frac{\alpha_{g1,max}^{1/3}\alpha_{g1}^{1/3}}{\alpha_{g1,max}^{1/3}-\alpha_{g1}^{1/3}}\right)\right] \times \left(1+\frac{10.3G}{R_{m2}}\right) \tag{B.5}$$

$$\phi_{RC}^{(2)} = -13.6 C_{RC}^{(2)}\varepsilon^{1/3}\frac{\alpha_{g2}^{2}}{W^{2}G}R_{m2}^{4/3}\left[1-\exp\left(-C_{RC2}\alpha_{g2}^{1/2}\right)\right] \times \left(1-2.0R_{c}^{*2}+\frac{9.0G}{R_{m2}}\right) \tag{B.6}$$

$$\eta_{RC,2}^{(11,2)} = 3.4 C_{RC}^{(1)}\frac{\varepsilon^{1/3}\alpha_{g1}^{2}a_{i1}^{2/3}}{\alpha_{g1,max}^{2/3}}\left[1-\exp\left(-C_{RC1}\frac{\alpha_{g1,max}^{1/3}\alpha_{g1}^{1/3}}{\alpha_{g1,max}^{1/3}-\alpha_{g1}^{1/3}}\right)\right] \times \left(1-\frac{2}{3}D_{c1}^{*}\right) \tag{B.7}$$

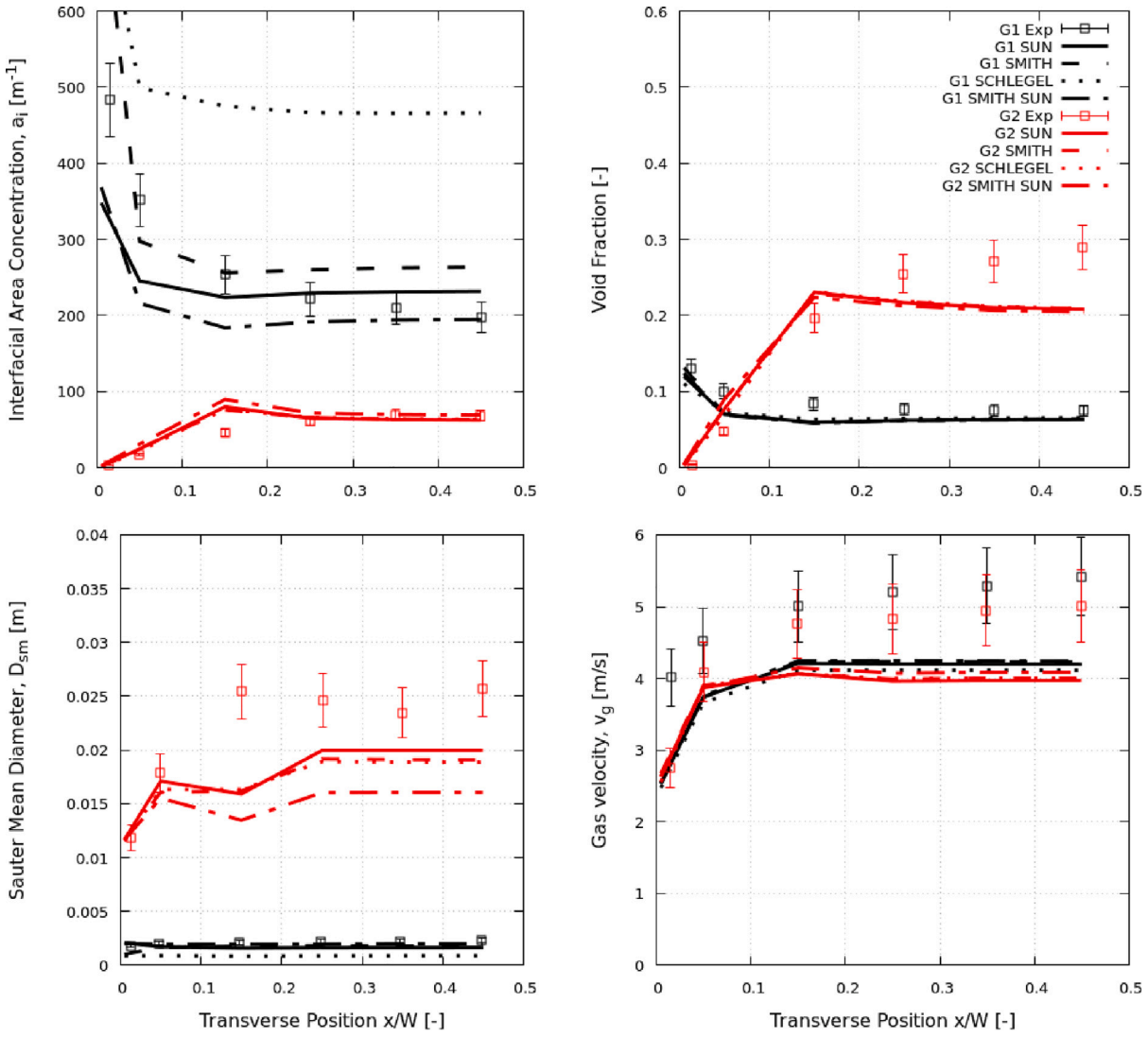

Fig. 18. Benchmark of line-averaged predicted results against experimental data at $z/D = 142$ for a churn-turbulent flow regime: interfacial area concentration, void fraction, Sauter mean diameter, gas velocity.

$$\eta_{RC,2}^{(12,2)} = 4.85 C_{RC}^{(12,2)} \varepsilon^{1/3} \frac{\alpha_{g1}^{5/3}\alpha_{g2}^{2}}{R_{m2}^{2/3}} \left[1 - \exp\left(-C_{RC1} \frac{\alpha_{g1,max}^{1/3}\alpha_{g1}^{1/3}}{\alpha_{g1,max}^{1/3} - \alpha_{g1}^{1/3}}\right)\right] \times \left(1 - (R_c^*)^{10/3}\right) \tag{B.8}$$

$C_{RC}^{(1)}$, $C_{RC}^{(12,2)}$, $C_{RC}^{(2)}$ are empirically determined coefficients.

- Wake Entrainment WE

The source/sink terms for wake entrainment required the following variables:

C_{D2} is the drag coefficient for the leading Group-2 bubble:

$$C_{D2} = \frac{8}{3}(1-\alpha_g)^2 = \frac{8}{3}(1-(\alpha_{g1}+\alpha_{g2}))^2 \tag{B.9}$$

u_{r1} is the relative velocity respectively for the leading Group-1 bubble.

The source/sink terms modelling the Wake Entrainment (WE) process are:

$$\phi_{WE}^{(1)} = -0.27 C_{WE}^{(1)} C_{D1}^{1/3} u_{r1} a_{i1}^2 \tag{B.10}$$

$$\phi_{WE,2}^{(11,2)} = 1.08 C_{WE}^{(11,2)} C_{D1}^{1/3} u_{r1} \frac{\alpha_{g1} a_{i1}}{G} \left(1 - \frac{2}{3} D_{c1}^*\right) \times \left[1 + 0.7 G^{7/6} \left(\frac{a_{i1}}{\alpha_1}\right)^{1/2} \left(\frac{\sigma}{g\Delta\rho}\right)^{-1/3}\right] \tag{B.11}$$

$$\phi_{WE,l1}^{(12,2)} = -4.35 C_{WE}^{(12,2)} \sqrt{g C_{D2} G} \frac{a_{i1}\alpha_{g2}}{R_{m2}} \tag{B.12}$$

$$\phi_{WE,g2}^{(12,2)} = 26.1 C_{WE}^{(12,2)} \frac{\alpha_{g1}\alpha_{g2}}{R_{m2}} \sqrt{\frac{g C_{D2}}{G}} \left(1 + 4.31 \frac{G}{R_{m2}}\right) \tag{B.13}$$

$$\phi_{WE}^{(2)} = -15.9 C_{WE}^{(2)} \frac{\alpha_{g2}^2}{R_{m2}^2} \sqrt{C_{D2} g G} \left(1 + 0.51 R_c^*\right) \tag{B.14}$$

$$\eta_{WE,2}^{(11,2)} = 5.40 C_{WE}^{(11,2)} C_{D1}^{1/3} u_{r1} \alpha_{g1} a_{i1} \left(1 - \frac{2}{3} D_{c1}^*\right) \tag{B.15}$$

$$\eta_{WE,2}^{(12,2)} = 4.35 C_{WE}^{(12,2)} \sqrt{g C_{D2} G} \frac{\alpha_{g1}\alpha_{g2}}{R_{m2}} \tag{B.16}$$

$C_{WE}^{(1)}$, $C_{WE}^{(11,2)}$, $C_{WE}^{(12,2)}$, $C_{WE}^{(2)}$ are empirically determined coefficients.

- Turbulent Impact TI

The source/sink terms modelling the Turbulent Impact (TI) process are:

$$\phi_{TI}^{(1)} = 0.12 C_{TI}^{(1)} \varepsilon^{1/3} \left(1 - \alpha_g\right) \left(\frac{a_{i1}^{5/3}}{\alpha_{g1}^{2/3}}\right) \exp\left(-\frac{We_{cr1}}{We_1}\right) \sqrt{1 - \frac{We_{cr1}}{We_1}} \tag{B.17}$$

$$\phi_{TI,1}^{(2,1)} = 2.71 C_{TI}^{(2)} \varepsilon^{1/3} \alpha_{g2} \left(1 - \alpha_g\right) \frac{G^{2/3} R_c^{*5/3} \left(1 - R_c^{*5/3}\right)}{R_{m2}^{7/3}}$$

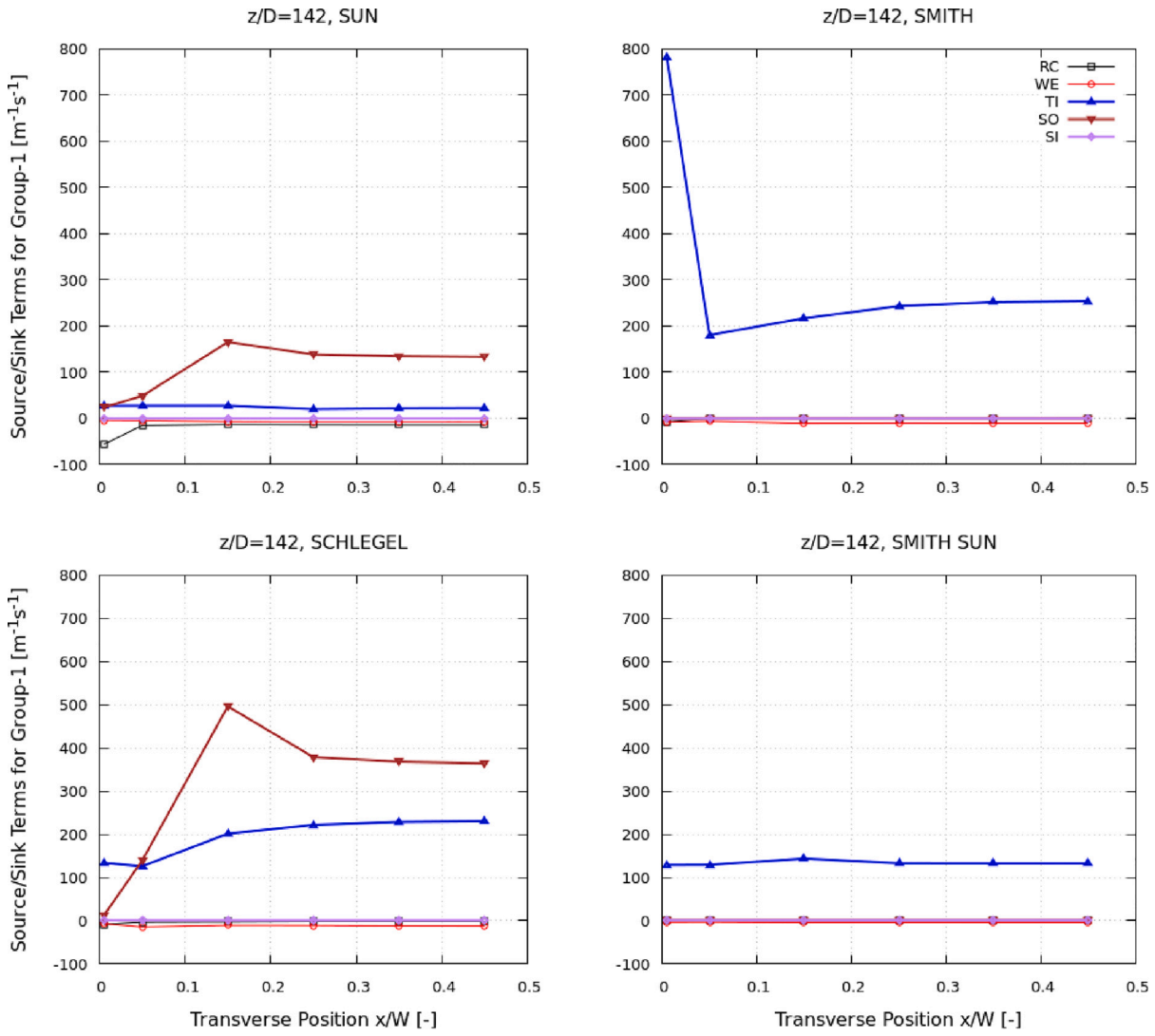

Fig. 19. Comparison of line-averaged coalescence/breakup mechanisms for Group-1 bubbles for SUN, SMITH, SCHLEGEL and SMITH-SUN terms at z/D = 142.

$$\times \exp\left(-\frac{We_{cr2}}{We_2}\right)\sqrt{1-\frac{We_{cr2}}{We_2}} \tag{B.18}$$

$$\phi_{TI,2}^{(2)} = 1.4C_{TI}^{(2)}\varepsilon^{1/3}\alpha_{g2}\left(1-\alpha_g\right)\left(\frac{G}{R_{m2}^{8/3}}\right)\exp\left(-\frac{We_{cr2}}{We_2}\right)$$

$$\times\sqrt{1-\frac{We_{cr2}}{We_2}}\left(1-2R_c^*\right) \tag{B.19}$$

$$\eta_{TI,2}^{(2,1)} = 0.34C_{TI}^{(2)}\varepsilon^{1/3}\alpha_{g2}\left(1-\alpha_g\right)\frac{GR_c^{*7/3}\left(1-R_c^{*5/3}\right)}{R_{m2}^{5/3}}$$

$$\times \exp\left(-\frac{We_{cr2}}{We_2}\right)\sqrt{1-\frac{We_{cr2}}{We_2}} \tag{B.20}$$

$$\eta_{TI,1}^{(2,1)} = -\eta_{TI,2}^{(2,1)} \tag{B.21}$$

$C_{TI}^{(1)}$, $C_{TI}^{(2)}$, We_{cr1}, We_{cr2} are empirically determined coefficients.

- Shearing-off (SO)

The source/sink terms modelling the Shearing-off (SO) process are:

$$\phi_{SO,1}^{(2,12)} = 64.51C_{SO}C_d^2\frac{\alpha_{g2}v_{rb}}{GR_{m2}}\left[1-\left(\frac{We_{c,SO}}{We_{m2}}\right)^3\right] \tag{B.22}$$

$$\phi_{SO,2}^{(2,12)} = -21.50C_{SO}C_d^3\left(\frac{\sigma}{\rho_f}\right)^{3/5}\frac{\alpha_{g2}}{v_{rb}^{1/5}G^{8/5}R_{m2}}\left[1-\left(\frac{We_{c,SO}}{We_{m2}}\right)^3 + \frac{3.24G}{R_{m2}}\left(1-\left(\frac{We_{c,SO}}{We_{m2}}\right)^2\right)\right] \tag{B.23}$$

$$\eta_{SO,2}^{(2,12)} = -10.75C_{SO}C_d^3\left(\frac{\sigma}{\rho_f G}\right)^{3/5}\frac{\alpha_{g2}}{v_{rb}^{1/5}R_{m2}}\left[1-\left(\frac{We_{c,SO}}{We_{m2}}\right)^3\right] \tag{B.24}$$

$$\eta_{SO,1}^{(2,12)} = -\eta_{SO,2}^{(2,12)} \tag{B.25}$$

C_{SO}, C_d are empirically determined coefficients.

- Surface Instability SI

The source/sink terms modelling the Surface Instability (SI) process are:

$$\phi_{SI}^{(2)} = 1.25\alpha_{g2}^2\left(\frac{\sigma}{g\Delta\rho}\right)^{-1}C_{RC}^{(2)}\varepsilon^{1/3}\frac{1}{W^2}\left(\frac{\sigma}{g\Delta\rho}\right)^{7/6} \times\left[1-\exp\left(-C_{RC2}\alpha_{g2}^{1/2}\right)\right] \tag{B.26}$$

$$+\ 2.875\times10^{-4}\alpha_{g2}^2\left(\frac{\sigma}{g\Delta\rho}\right)^{-1}C_{WE}^{(2)}\sqrt{C_{D2}gG} \tag{B.27}$$

$C_{RC}^{(2)}$ and $C_{WE}^{(2)}$ are empirically determined coefficients.

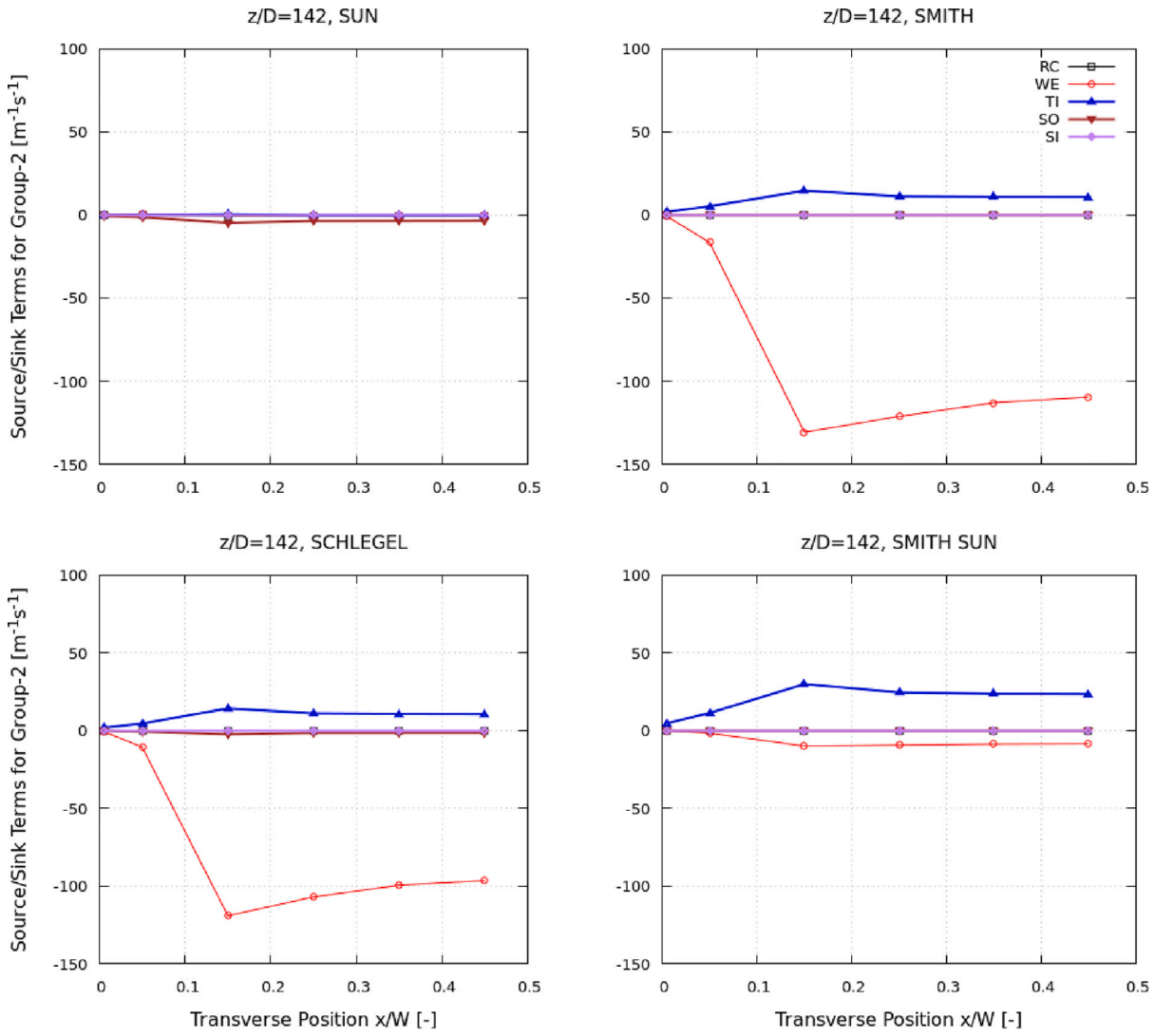

Fig. 20. Comparison of line-averaged coalescence/breakup mechanisms for Group-2 bubbles for SUN, SMITH, SCHLEGEL and SMITH-SUN terms at z/D = 142.

- Others coefficients

$$R_c = D_c/2 \tag{B.28}$$

$$D^*_{cj} = D_c/D_{smj} \quad j = 1,2 \tag{B.29}$$

$$R^*_c = R_c/R_{m2} \tag{B.30}$$

R_{m2} is the radius of curvature of the maximum bubble in the system. For the experiment of (Sun, 2001),

$$R_{m2} = 1.915 D_{sm2} \tag{B.31}$$

$$We_1 = \frac{2\rho_f \overline{u}^2_{t1} D_{sm1}}{\sigma} = \frac{2\rho_f \varepsilon^{1/3} D^{5/3}_{sm1}}{\sigma} \tag{B.32}$$

$$We_{m2} = \frac{2\rho_f v^2_{rb} R_{m2}}{\sigma} \tag{B.33}$$

v_{rb} is the relative velocity of the large bubble with respect to the liquid film near the cap bubble base. It is estimated by the velocity of Group-2 bubbles in the main flow direction. D_{sm1} and D_{sm2} are the Sauter mean diameter respectively for Group-1 and Group-2 bubbles.

Appendix C. Coalescence/breakup terms proposed by Smith et al. (2012b) and Schlegel et al. (2015)

The terms proposed by Smith and al. for large diameter pipes are listed in the following.

- Random collision RC

The source/sink terms modelling the Random Collision (RC) process are:

$$\phi^{(1)}_{RC} = -0.17 C^{(1)}_{RC} \lambda^{(1)}_{RC} \frac{\varepsilon^{1/3} \alpha_{g1} a^{5/3}_{i1}}{\alpha^{1/3}_{g1,max}\left(\alpha^{1/3}_{g1,max} - \alpha^{1/3}_{g1}\right)} \times \left[1 - \exp\left(-C_{RC1} \frac{\alpha^{1/3}_{g1,max}\alpha^{1/3}_{g1}}{\alpha^{1/3}_{g1,max} - \alpha^{1/3}_{g1}}\right)\right] \tag{C.1}$$

$$\phi^{(11,2)}_{RC,2} = 4.1 C^{(1)}_{RC} \lambda^{(1)}_{RC} \frac{\varepsilon^{1/3} \alpha_{g1} a^{5/3}_{i1}}{\alpha^{2/3}_{g1,max}} \left[1 - \exp\left(-C_{RC1} \frac{\alpha^{1/3}_{g1,max}\alpha^{1/3}_{g1}}{\alpha^{1/3}_{g1,max} - \alpha^{1/3}_{g1}}\right)\right] \times \left(1 - \frac{2}{3} D^*_{c1}\right) \tag{C.2}$$

$$\phi^{(12,2)}_{RC,1} = -1.14 C^{(12,2)}_{RC} \lambda^{(12,2)}_{RC} \varepsilon^{1/3} \alpha^{2/3}_{g1} \alpha^{4/3}_{g2} a_{i1} a^{2/3}_{i2} \times \left[1 - \exp\left(-C_{RC1} \frac{\alpha^{1/3}_{g1,max}\alpha^{1/3}_{g1}}{\alpha^{1/3}_{g1,max} - \alpha^{1/3}_{g1}}\right)\right] \tag{C.3}$$

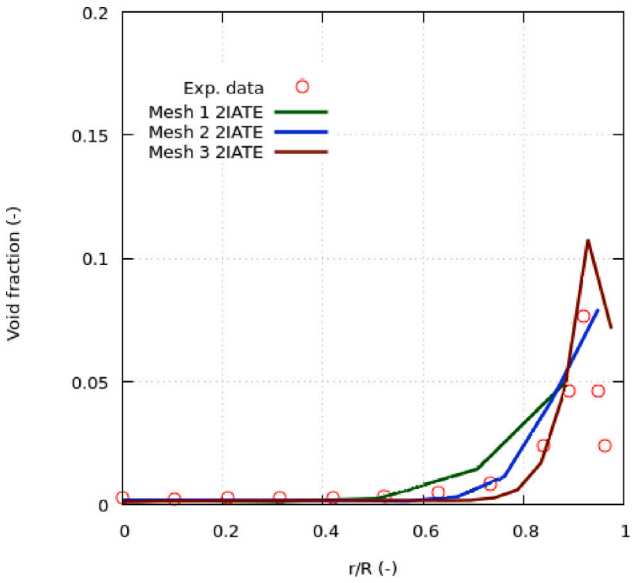

Fig. 21. Void fraction distribution.

$$\phi_{RC,2}^{(12,2)} = 1.80 C_{RC}^{(12,2)} \lambda_{RC}^{(12,2)} \varepsilon^{1/3} \alpha_{g1}^{5/3} \alpha_{g2}^{1/3} a_{i2}^{5/3} \times \left[1 - \exp\left(-C_{RC1} \frac{\alpha_{g1,max}^{1/3} \alpha_{g1}^{1/3}}{\alpha_{g1,max}^{1/3} - \alpha_{g1}^{1/3}}\right)\right] \tag{C.4}$$

$$\phi_{RC}^{(2)} = -95.7 C_{RC}^{(2)} \lambda_{RC}^{(2)} \varepsilon^{1/3} \frac{\alpha_{g2}^{7/3}}{D_h^2} \frac{1}{a_{i2}^{1/3}} \left[1 - \exp\left(-C_{RC2} \alpha_{g2}^{1/2}\right)\right] \times \left(1 - 0.37 D_{c2}^{*3}\right) \tag{C.5}$$

$$\eta_{RC,2}^{(11,2)} = 3.15 C_{RC}^{(1)} \lambda_{RC}^{(1)} \frac{\varepsilon^{1/3} \alpha_{g1}^2 a_{i1}^{2/3}}{\alpha_{g1,max}^{2/3}} \left[1 - \exp\left(-C_{RC1} \frac{\alpha_{g1,max}^{1/3} \alpha_{g1}^{1/3}}{\alpha_{g1,max}^{1/3} - \alpha_{g1}^{1/3}}\right)\right] \times \left(1 - \frac{2}{3} D_{c1}^{*}\right) \tag{C.6}$$

$$\eta_{RC,2}^{(12,2)} = 1.44 C_{RC}^{(12,2)} \lambda_{RC}^{(12,2)} \varepsilon^{1/3} \alpha_{g1}^{5/3} \alpha_{g2}^{4/3} a_{i2}^{2/3} \times \left[1 - \exp\left(-C_{RC1} \frac{\alpha_{g1,max}^{1/3} \alpha_{g1}^{1/3}}{\alpha_{g1,max}^{1/3} - \alpha_{g1}^{1/3}}\right)\right] \tag{C.7}$$

$\lambda_{RC}^{(1)}$, $\lambda_{RC}^{(12,2)}$, $\lambda_{RC}^{(2)}$ are defined as follows:

$$\lambda_{RC}^{(1)} = \exp\left(-C_{RC0} \frac{D_{sm1}^{5/6} \rho_f^{1/2} \varepsilon^{1/3}}{\sigma^{1/2}}\right) \tag{C.8}$$

$$\lambda_{RC}^{(2)} = \exp\left(-C_{RC0} \frac{D_{sm2}^{5/6} \rho_f^{1/2} \varepsilon^{1/3}}{\sigma^{1/2}}\right) \tag{C.9}$$

$$\lambda_{RC}^{(12,2)} = \lambda_{RC}^{(2)} \tag{C.10}$$

In the above equations, $C_{RC}^{(1)}$, $C_{RC}^{(12,2)}$, $C_{RC}^{(2)}$ are three constant coefficients. C_{RC1}, C_{RC2} are coefficients accounting for effective range of influence of turbulent eddies. $\alpha_{g1,max}$ is the dense packing limit for Group 1 bubbles. D_h is the hydraulic diameter. C_{RC0} is a constant coefficient.

- $C_{RC}^{(1)} = 0.01$, $C_{RC}^{(12,2)} = 0.01$, $C_{RC}^{(2)} = 0.01$.
- $C_{RC1} = 3.0$, $C_{RC2} = 3.0$
- $\alpha_{g1,max} = 0.62$
- $C_{RC0} = 3.0$

- Wake entrainment WE

The source/sink terms modelling the Wake Entrainment (WE) process are:

$$\phi_{WE}^{(1)} = -0.17 C_{WE}^{(1)} C_{D1}^{1/3} u_{r1} a_{i1}^2 \tag{C.11}$$

$$\phi_{WE,2}^{(11,2)} = 2.57 C_{WE}^{(11,2)} C_{D1}^{1/3} u_{r1} a_{i1}^2 \left(1 - \frac{2}{3} D_{c1}^{*}\right) \tag{C.12}$$

$$\phi_{WE,l1}^{(12,2)} = -0.33 C_{WE}^{(12,2)} \overline{u}_{w12} a_{i1} a_{i2} \tag{C.13}$$

$$\phi_{WE,g2}^{(12,2)} = 0.922 C_{WE}^{(12,2)} \overline{u}_{w12} \alpha_{g1} \frac{a_{i2}^2}{\alpha_{g2}} \tag{C.14}$$

$$\phi_{WE}^{(2)} = -1.02 C_{WE}^{(2)} \left[1 - \exp(-0.7\alpha_{g2})\right] \overline{u}_{rw2} \frac{a_{i2}^2}{\alpha_{g2}} \left(1 - 0.10 D_{c2}^{*2}\right) \tag{C.15}$$

$$\eta_{WE,2}^{(11,2)} = 3.85 C_{WE}^{(1)} C_{D1}^{1/3} u_{r1} \alpha_{g1} a_{i1} \left(1 - \frac{2}{3} D_{c1}^{*}\right) \tag{C.16}$$

$$\eta_{WE,2}^{(12,2)} = 0.33 C_{WE}^{(12,2)} \overline{u}_{w12} \alpha_{g1} a_{i2} \tag{C.17}$$

In the above equation

$$\overline{u}_{rw2} = 0.94 u_{r2} C_{D2}^{1/3}$$

$$\overline{u}_{w12} = \overline{u}_{rw2} + u_{r1} - u_{r2}$$

$$D_{c2}^{*} = \frac{D_c}{D_{sm2}}$$

and

$$C_{D1} = \frac{2}{3} D_{sm1} \sqrt{\frac{g\Delta\rho}{\sigma}} \left(\frac{1 + 17.67[f(\alpha_{g1})]^{6/7}}{18.67 f(\alpha_{g1})}\right)^2 \text{ with}$$

$$f(\alpha_{g1}) = (1 - \alpha_{g1})^{1.5}$$

$$C_{D2} = \frac{8}{3}(1 - \alpha_{g2})^2$$

In the above equations $C_{WE}^{(1)}$, $C_{WE}^{(11,2)}$, $C_{WE}^{(12,2)}$, $C_{WE}^{(2)}$ are constant coefficients.

- $C_{WE}^{(1)} = 0.002$, $C_{WE}^{(12,2)} = 0.01$, $C_{WE}^{(2)} = 0.06$ (in Smith et al., 2012a,b)
- $C_{WE}^{(1)} = 0.01$, $C_{WE}^{(12,2)} = 0.02$, $C_{WE}^{(2)} = 0.05$ (in Schlegel et al., 2015)
- $C_{WE}^{(1)} = 0.002$, $C_{WE}^{(11,2)} = 0.002$, $C_{WE}^{(12,2)} = 0.02$, $C_{WE}^{(2)} = 0.05$ in Lee et al. (2013)
- $C_{D1} = \frac{2}{3} D_{sm1} \sqrt{\frac{g\Delta\rho}{\sigma}} (1 - \alpha_{g1} - \alpha_{g2})^{-0.5}$ in Schlegel et al. (2015)

- Turbulent impact TI

The source/sink terms modelling the Turbulent Impact (TI) process are:

$$\phi_{TI}^{(1)} = 0.12 C_{TI}^{(1)} \varepsilon^{1/3} (1 - \alpha_g) \left(\frac{a_{i1}^{5/3}}{\alpha_{g1}^{2/3}}\right) \exp\left(-\frac{We_{cr1}}{We_1}\right) \sqrt{1 - \frac{We_{cr1}}{We_1}} \tag{C.18}$$

$$\phi_{TI,1}^{(2,1)} = 6.165 C_{TI}^{(2,1)} \varepsilon^{1/3} (1 - \alpha_g) \left(\frac{a_{i2}^{5/3}}{\alpha_{g2}^{2/3}}\right) \exp\left(-\frac{We_{cr2}}{We_2}\right) \sqrt{1 - \frac{We_{cr2}}{We_2}} \times \left(0.212 D_{c2}^{*13/3} - 0.167 D_{c2}^{*5}\right) \tag{C.19}$$

$$\phi_{TI,2}^{(2)} = 0.378 C_{TI}^{(2)} \varepsilon^{1/3} (1 - \alpha_g) \left(\frac{a_{i2}^{5/3}}{\alpha_{g2}^{2/3}}\right) \exp\left(-\frac{We_{cr2}}{We_2}\right) \sqrt{1 - \frac{We_{cr2}}{We_2}} \times \left(1 - 0.212 D_{c2}^{*13/3}\right) \tag{C.20}$$

$$\eta_{TI,2}^{(2,1)} = -11.65 C_{TI}^{(2,1)} \varepsilon^{1/3} (1 - \alpha_g) \alpha_{g2}^{1/3} a_{i2}^{2/3} \exp\left(-\frac{We_{cr2}}{We_2}\right) \times \sqrt{1 - \frac{We_{cr2}}{We_2}} \left(0.15 D_{c2}^{*16/3} - 0.117 D_{c2}^{*6}\right) \tag{C.21}$$

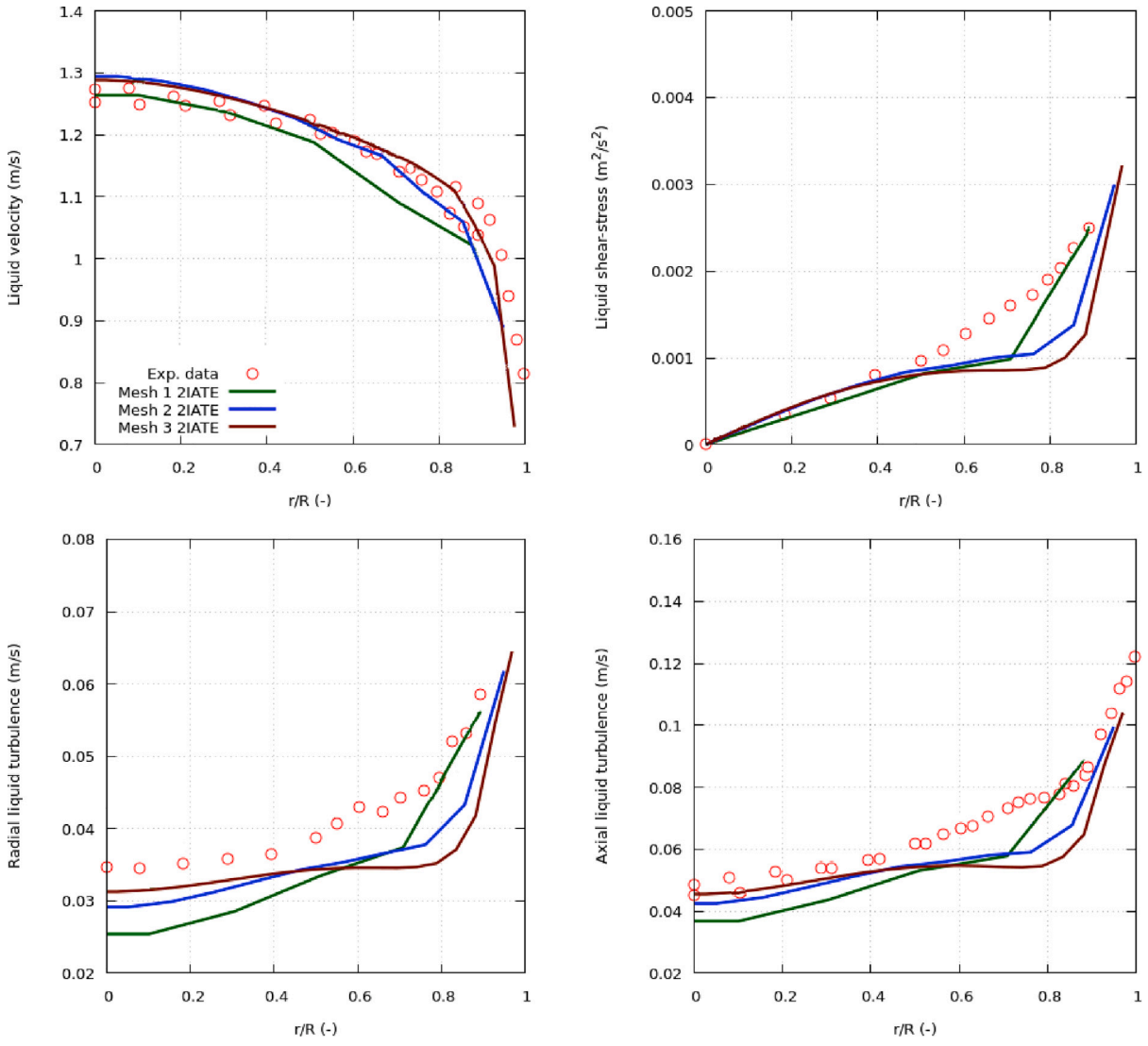

Fig. 22. Liquid-phase velocity and turbulent quantities.

$$\eta_{TI,1}^{(2,1)} = -\eta_{TI,2}^{(2,1)} \tag{C.22}$$

with the following expressions for We_1 and We_2

$$We_1 = \frac{2\rho_f \epsilon^{2/3} (D_{sm1})^{5/3}}{\sigma}$$
$$We_2 = \frac{2\rho_f \epsilon^{2/3} (D_{sm2})^{5/3}}{\sigma}$$

$C_{TI}^{(1)}$, $C_{TI}^{(2,1)}$, $C_{TI}^{(2)}$ are constant coefficients. We_{cr1}, We_{cr2} are critical Weber number for breakup due to turbulent impact.

- $C_{TI}^{(1)} = 0.05$, $C_{TI}^{(2,1)} = 0.04$, $C_{TI}^{(2)} = 0.01$ in Smith et al. (2012a,b)
- $C_{TI}^{(1)} = 0.1$, $C_{TI}^{(2,1)} = 0.02$, $C_{TI}^{(2)} = 0.02$ in Lee et al. (2013)
- $We_{cr1} = 1.2$, $We_{cr2} = 1.2$ in Smith et al. (2012a,b)
- $We_{c,TI1} = 6.5$, $We_{c,TI2} = 7.0$ in Lee et al. (2013)

- Shearing-off SO

The source/sink terms modelling the Shearing-off (SO) process are:

$$\phi_{SO,1}^{(2,12)} = 8.0 C_{SO} \frac{\rho_f^{3/5} v_{g2}^{1/5} \sigma^{2/5}}{\rho_g D_h^{2/5} We_c^{3/5}} \frac{a_{i2}^2}{\alpha_{g2}} \left[1 - \left(\frac{We_{c,SO}}{We_{m2}}\right)^4\right] \tag{C.23}$$

$$\phi_{SO,2}^{(2,12)} = -0.36 C_{SO} \left(\frac{\sigma}{\rho_g v_{g2}}\right) \frac{a_{i2}^3}{\alpha_{g2}^2} \left[1 - \left(\frac{We_{c,SO}}{We_{m2}}\right)\right] \tag{C.24}$$

$$\eta_{SO,2}^{(2,12)} = -2.33 C_{SO} \left(\frac{\sigma}{\rho_g v_{g2}}\right) \frac{a_{i2}^2}{\alpha_{g2}} \left[1 - \left(\frac{We_{c,SO}}{We_{m2}}\right)^4\right] \tag{C.25}$$

$$\eta_{SO,1}^{(2,12)} = -\eta_{SO,2}^{(2,12)} \tag{C.26}$$

Schlegel et al. proposed the following term

$$\phi_{SO,1}^{(2,12)} = 7.17 C_{SO} \frac{\rho_f^{3/5} v_{r1}^{1/5} \sigma^{2/5}}{\rho_g D_h^{2/5}} \frac{a_{i2}^2}{\alpha_{g2}} \left[1 - \left(\frac{We_{c,SO}}{We_{m2}}\right)^4\right] \tag{C.27}$$

C_{SO} is a constant coefficient. $We_{c,SO}$ is a critical weber number for shearing-off of small bubbles from large cap bubbles. We_{m2}, We_c, D_h.

- $C_{SO} = 2.5 \times 10^{-6}$, $We_{c,SO} = 4000$ (in Smith et al., 2012a,b)
- $C_{SO} = 5 \times 10^{-5}$, $We_{c,SO} = 10$ (in Schlegel et al., 2015)
- $C_{SO} = 3.8 \times 10^{-5}$, $We_{c,SO} = 4500$, $C_d = 4.8$ (in Lee et al., 2013)

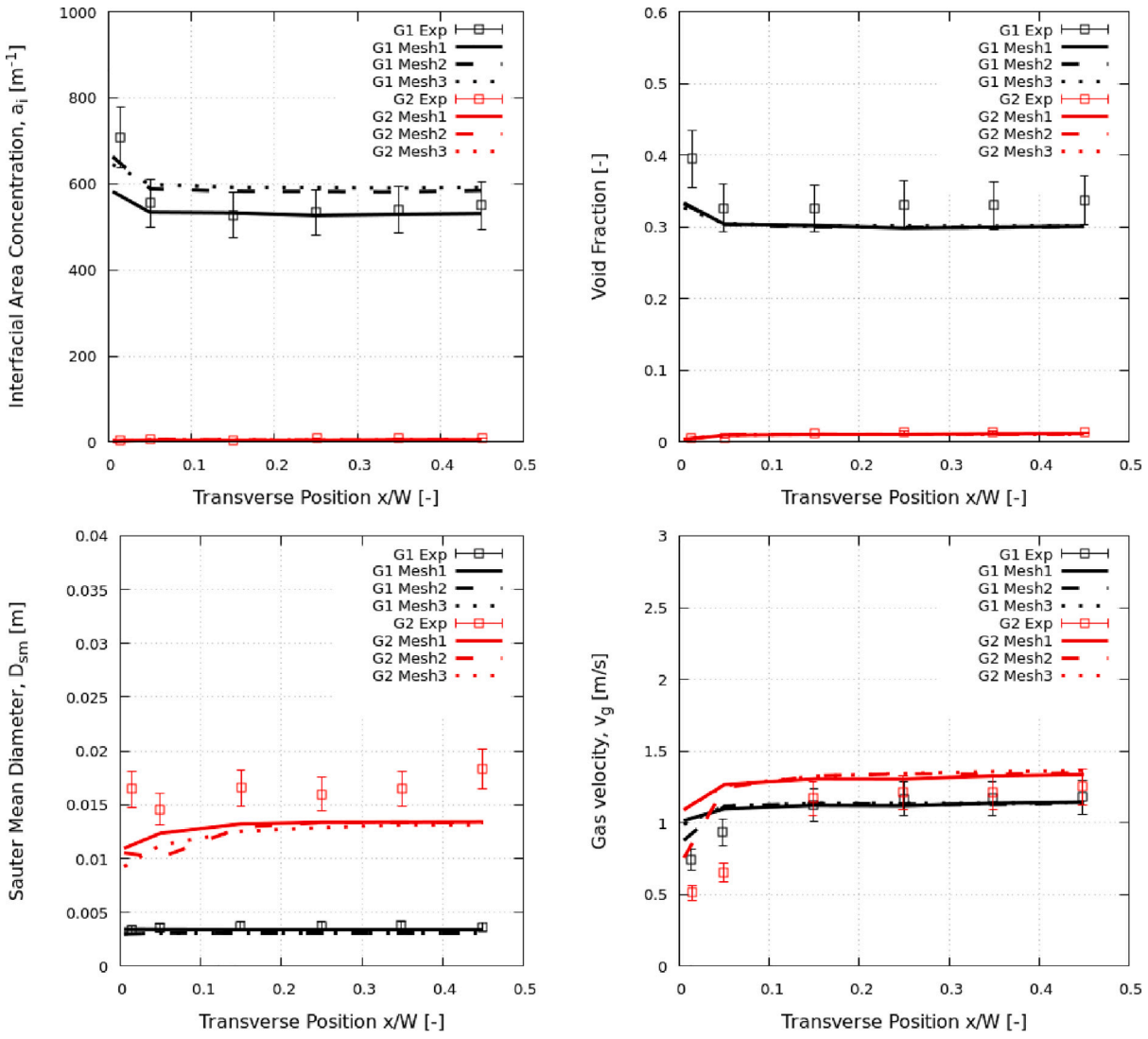

Fig. D.23. Cap-bubbly: benchmark between the three meshes and experimental data at z/D = 142.

- Surface instability SI

The source/sink terms modelling the Surface Instability (SI) process are:

$$\phi_{SI}^{(2)} = 2.616\times10^{-4} C_{RC}^{(2)} \varepsilon^{1/3} \frac{1}{D_h^2} \alpha_{g2}^2 \left(\frac{\sigma}{g\Delta\rho}\right)^{1/6} \times \left[1-\exp\left(-C_{RC2}\alpha_{g2}^{1/2}\right)\right] \quad \text{(C.28)}$$

$$+\ 1.425\times10^{-7} C_{WE}^{(2)} P_{WE}^{(2)} \bar{u}_{rw2} \alpha_{g2}^2 \left(\frac{\sigma}{g\Delta\rho}\right)^{-1} \quad \text{(C.29)}$$

Schlegel et al. proposed the following term:

$$\phi_{SI}^{(2)} = 2.616\times10^{-4} C_{RC}^{(2)} \varepsilon^{1/3} \frac{1}{D_h^2} \alpha_{g2}^2 \left(\frac{\sigma}{g\Delta\rho}\right)^{1/6} \times \left[1-\exp\left(-C_{RC2}\alpha_{g2}^{1/2}\right)\right] \quad \text{(C.30)}$$

$$+\ 1.425\times10^{-7} C_{WE}^{(2)} (1-\exp(-0.7\alpha_{g2})) \bar{u}_{rw2} \alpha_{g2}^2 \left(\frac{\sigma}{g\Delta\rho}\right)^{-1} \quad \text{(C.31)}$$

$C_{RC}^{(2)}$ and $C_{WE}^{(2)}$ are constant coefficients. D_h is the hydraulic diameter.

- $C_{RC}^{(2)} = 0.01$, $C_{WE}^{(2)} = 0.06$ (in Smith et al., 2012a,b)
- $C_{RC}^{(2)} =$, $C_{WE}^{(2)} = 0.05$ (in Schlegel et al., 2015)
- $C_{RC}^{(2)} = 0.005$, $C_{WE}^{(2)} = 0.005$ (in Lee et al., 2013)

Appendix D. Other results

D.1. Mesh sensitivity

Comparison at $Z/D = 142$ shows the same results as those already shown in Section 4.2.1, supporting the conclusion that mesh 2 can be used for all simulations.

References

Beyer, M., Lucas, D., Kussin, J., Schütz, P., 2008. Air water experiments in a vertical DN200-pipe.

Bois, G., 2017. Direct numerical simuation of a turbulent bubbly flow in a vertical channel: towards an improved second-order Reynolds stress model. Nucl. Eng. Des. 321, 92–103.

Burns, A., Grank, T., Hamill, I., Shi, J.-M., 2004. The favre averaged drag model for turbulent dispersion in Eulerian multi-phase flows. In: 5th International Conference on Multiphase Flow, ICMF, Yokohama, Japan.

Coste, P., 2013. A large interface model for two-phase CFD. Nucl. Eng. Des. 255, 38–50. http://dx.doi.org/10.1016/j.nucengdes.2012.10.008.

Doup, B., 2014. Methodology Development of a Gas-Liquid Dynamic Flow Regime Transition Model (PhD Dissertation). The Ohio State University.

du Cluzeau, A., Bois, G., Toutant, A., 2019. Analysis and modeling of Reynolds stress in turbulent bubbly up-flows from Direct numerical simulations. J. Fluid Mech. 866, 132–168.

du Cluzeau, A., Bois, G., Toutant, A., 2020a. Modelling on the laminar dispersion force in bubbly flows from direct numerical simulations. Phys. Fluids 32.

du Cluzeau, A., Bois, G., Toutant, A., Martinez, J.-M., 2020b. On bubble forces in turbulent channel flows from direct numerical simulations. J. Fluid Mech. 882.

EDF, CEA, FRAMATOME, IRSN, Code_Saturne. URL https://www.code-saturne.org/cms/web/NEPTUNECFD.

Frank, T., Zwart, P.J., Krepper, E., Prasser, H.M., Lucas, D., 2008. Validation of CFD models for mono- and polydisperse air-water two-phase flows in pipes. Nucl. Eng. Des. 238 (3), 647–659. http://dx.doi.org/10.1016/j.nucengdes.2007.02.056.

Fu, X.Y., Ishii, M., 2003. Two-group interfacial area transport in vertical air-water flow - I. Mechanistic model. Nucl. Eng. Des. 219 (2), 143–168. http://dx.doi.org/10.1016/S0029-5493(02)00285-6.

Gürkan, T., Wellek, R.M., 1976. Mass transfer in dispersed and continous phases for creeping flow of fluid spheres through power law fluids. Industrial & Engineering Chemistry Fundamentals 15 (1), 45–52.

Hibiki, T., Ishii, M., 2000. Two-group interfacial area transport equations at bubbly-to-slug flow transition. Nucl. Eng. Des. 202 (1), 39–76. http://dx.doi.org/10.1016/S0029-5493(00)00286-7.

Ishii, M., Hibiki, T., 2006. Thermo-Fluid Dynamics of Two-Phase Flow. Springer, pp. 1–462. http://dx.doi.org/10.1007/978-0-387-29187-1, arXiv:arXiv:1011.1669v3.

Ishii, M., Kim, S., Uhle, J., 2002. Interfacial area transport equation: Model development and benchmark experiments. Int. J. Heat Mass Transfer 45 (15), 3111–3123. http://dx.doi.org/10.1016/S0017-9310(02)00041-8.

Ishii, M., Zuber, N., 1979. Drag coefficient and relative velocity in bubbly, droplet or particulate flows. AIChE J. 25 (5), 843–855. http://dx.doi.org/10.1002/aic.690250513.

Kim, S., Ishii, M., Kong, R., Wang, G., 2021. Progress in two-phase flow modeling: Interfacial area transport. Nucl. Eng. Des. 373, 111019. http://dx.doi.org/10.1016/j.nucengdes.2020.111019, URL https://www.sciencedirect.com/science/article/pii/S0029549320305136.

Kocamustafaogullari, G., Ishii, M., 1995. Foundation of the interfacial area transport equation and its closure relations. Int. J. Heat Mass Transfer 38 (3), 481–493. http://dx.doi.org/10.1016/0017-9310(94)00183-V.

Krepper, E., Beyer, M., Frank, T., Lucas, D., Prasser, H.M., 2009. CFD modelling of polydispersed bubbly two-phase flow around an obstacle. Nucl. Eng. Des. 239 (11), 2372–2381. http://dx.doi.org/10.1016/j.nucengdes.2009.06.015.

Krepper, E., Lucas, D., Frank, T., Prasser, H.M., Zwart, P.J., 2008. The inhomogeneous MUSIG model for the simulation of polydispersed flows. Nucl. Eng. Des. 238 (7), 1690–1702. http://dx.doi.org/10.1016/j.nucengdes.2008.01.004.

Krepper, E., Lucas, D., Prasser, H.M., 2005. On the modelling of bubbly flow in vertical pipes. Nucl. Eng. Des. 235 (5), 597–611. http://dx.doi.org/10.1016/j.nucengdes.2004.09.006.

Laviéville, J., Mérigoux, N., Guingo, M., Baudry, C., Mimouni, S., 2017. A generalized turbulent dispersion model for bubbly flow numerical simulation in NEPTUNE_CFD. Nucl. Eng. Des. 312, 284–293. http://dx.doi.org/10.1016/j.nucengdes.2016.11.003.

Lee, D.Y., Liu, Y., Hibiki, T., Ishii, M., Buchanan, J.R., 2013. A study of adiabatic two-phase flows using the two-group interfacial area transport equations with a modified two-fluid model. Int. J. Multiph. Flow. 57, 115–130. http://dx.doi.org/10.1016/j.ijmultiphaseflow.2013.07.008.

Liu, T.J., Bankoff, S.G., 1993. Structure of air-water bubbly flow in a vertical pipe-II. Void fraction, bubble velocity and bubble size distribution. Int. J. Heat Mass Transfer 36 (4), 1061–1072. http://dx.doi.org/10.1016/S0017-9310(05)80290-X.

Liu, Z., Li, L., Qi, F., et al., 2015. Population balance modeling of polydispersed bubbly flow in continuous-casting using multiple-size-group approach. Metall. Mater. Trans. B 46, 406–420.

Lopez De Bertodano, M.A., 1998. Two fluid model for two-phase turbulent jets. Nucl. Eng. Des. 179 (1), 65–74. http://dx.doi.org/10.1016/S0029-5493(97)00244-6.

Lucas, D., Beyer, M., Szalinski, L., Schütz, P., 2010. A new database on the evolution of air-water flows along a large vertical pipe. Int. J. Therm. Sci. 49 (4), 664–674. http://dx.doi.org/10.1016/j.ijthermalsci.2009.11.008.

Mérigoux, N., Laviéville, J., Mimouni, S., Guingo, M., Baudry, C., 2016. Reynolds stress turbulence model applied to two-phase pressurized thermal shocks in nuclear power plant. Nucl. Eng. Des. 299, 201–213. http://dx.doi.org/10.1016/j.nucengdes.2015.07.015.

Ozar, B., Brooks, C., Euh, D., Hibiki, T., Ishii, M., 2013. Investigation of one-dimensional interfacial area transport for vertical upward air–water two-phase flow in an annular channel at elevated pressures. Nucl. Eng. Des. 263, 362–379. http://dx.doi.org/10.1016/j.nucengdes.2013.05.018, URL https://www.sciencedirect.com/science/article/pii/S0029549313002811.

Prasser, H.-M., Beyer, M., Carl, H., Manera, A., Pietruske, H., Schütz, P., Weiß, F.-P., 2006. The multipurpose thermalehydraulic test facility TOPFLOW: an overview on experimental capabilities, instrumentation and results. Kerntechnik 71, 163–173.

Schaffrath, A., Krüssenberg, A.-K., Weiß, F.-P., Hicken, E.-F., Beyer, M., Carl, H., Prasser, H.-M., Schuster, J., Schütz, P., Tamme, M., 2001. TOPFLOW - a new multi-purpose thermalhydraulic test facility for the investigation of steady state and transient two-phase flow phenomena. Kerntechnik 66, 209–212.

Schlegel, J.P., Hibiki, T., Ishii, M., 2015. Two-group modeling of interfacial area transport in large diameter channels. Nucl. Eng. Des. 293, 75–86. http://dx.doi.org/10.1016/j.nucengdes.2015.07.011.

Schlegel, J.P., Sharma, S., Cuenca, R.M., Hibiki, T., Ishii, M., 2014. Local flow structure beyond bubbly flow in large diameter channels. Int. J. Heat Fluid Flow 47, 42–56. http://dx.doi.org/10.1016/j.ijheatfluidflow.2014.03.001.

Sharma, S.L., Ishii, M., Hibiki, T., Schlegel, J.P., Liu, Y., Buchanan, Jr., J.R., 2019. Beyond bubbly two-phase flow investigation using a CFD three-field two-fluid model. Int. J. Multiph. Flow. 113, 1–15.

Smith, T.R., Schlegel, J.P., Hibiki, T., Ishii, M., 2012a. Mechanistic modeling of interfacial area transport in large diameter pipes. Int. J. Multiph. Flow. 47 (2012), 1–16. http://dx.doi.org/10.1016/j.ijmultiphaseflow.2012.06.009.

Smith, T.R., Schlegel, J.P., Hibiki, T., Ishii, M., 2012b. Two-phase flow structure in large diameter pipes. Int. J. Heat Fluid Flow 33 (1), 156–167. http://dx.doi.org/10.1016/j.ijheatfluidflow.2011.10.008.

Sun, X., 2001. Two-Group Interfacial Area Transport Equation for a Confined Test Section (PhD Dissertation). Purdue University, p. 336.

Sun, X., Ishii, M., Kelly, J.M., 2003. Modified two-fluid model for the two-group interfacial area transport equation. Ann. Nucl. Energy 30 (16), 1601–1622. http://dx.doi.org/10.1016/S0306-4549(03)00150-6.

Sun, X., Kim, S., Cheng, L., Ishii, M., Beus, S.G., 2004a. Interfacial structures in confined cap-turbulent and churn-turbulent flows. Int. J. Heat Fluid Flow 25 (1), 44–57. http://dx.doi.org/10.1016/j.ijheatfluidflow.2003.08.001.

Sun, X., Kim, S., Ishii, M., Beus, S.G., 2004b. Model evaluation of two-group interfacial area transport equation for confined upward flow. Nucl. Eng. Des. 230 (1–3), 27–47. http://dx.doi.org/10.1016/j.nucengdes.2003.10.014.

Sun, X., Kim, S., Ishii, M., Beus, S.G., 2004c. Modeling of bubble coalescence and disintegration in confined upward two-phase flow. Nucl. Eng. Des. 230 (1–3), 3–26. http://dx.doi.org/10.1016/j.nucengdes.2003.10.008.

Tomiyama, A., Tamai, H., Zun, I., Hosokawa, S., 2002. Transverse migration of single bubbles in simple shear flows. Chem. Eng. Sci. 57 (11), 1849–1858. http://dx.doi.org/10.1016/S0009-2509(02)00085-4.

Wang, G., Ishii, M., 2021. Comprehensive evaluation of txo-group interfacial area transport equation and new intergroup transfer model. Int. J. Heat Mass Transfer 174, 121281.

Worosz, T., 2015. Interfacial Area Transport Equation for Bubbly to Cap-bubbly Transition Flows (PhD Dissertation). The Pennsylvania State University.

Yang, X., Schlegel, J., Liu, Y., Paranjape, S., Hibiki, T., Ishii, M., Bajorek, S., Ireland, A., 2016. Prediction of interfacial area transport in a scaled 8x8 BWR rod bundle. Nucl. Eng. Des. 310, 638–647. http://dx.doi.org/10.1016/j.nucengdes.2016.10.037, URL https://www.sciencedirect.com/science/article/pii/S0029549316304149.

Zuber, N., 1964. On the dispersed two-phase flow in the laminar flow regime. Chem. Eng. Sci. 19 (11), 897–917. http://dx.doi.org/10.1016/0009-2509(64)85067-3, URL http://www.sciencedirect.com/science/article/pii/0009250964850673.